• U C •

FCTUC FACULDADE DE CIÊNCIAS
E TECNOLOGIA
UNIVERSIDADE DE COIMBRA

Ana Carolina Pinto da Silveira

Extended Biomechanical Model of the Ankle-Foot Complex: Incorporation of Muscles and Ligaments

Thesis submitted for the degree of Master in Biomedical Engineering

Thesis Supervisors:

Prof. Dr. Ilse Jonkers (Dept. of Kinesiology, KU Leuven)
Prof. Dr. Maria Augusta Neto (Dept. of Mechanical Engineering, University of Coimbra)
Dennis Vandenbussche (RS Print, Paal, Belgium)

Assessor:

Prof. Josef Vander Sloten (Dept. of Mechanical Engineering, KU Leuven)

Mentors:

Wouter Aerts (Dept. of Mechanical Engineering, KU Leuven)
Tiago Malaquias (Dept. of Mechanical Engineering, KU Leuven)

Coimbra, 2015

Master thesis developed in cooperation with:

Preface

The moment of finishing my master thesis marks the end of the most challenging and fulfilling ride so far. The past five years have been a tremendous experience, that would not be possible if not being surrounded by incredible people.

I want to express my most sincere gratitude to professor Ilse Jonkers. Thank you for showing me what true guidance, trust and support are. Thank you for integrating me so well in the team, for always caring so much and for making this experience so remarkable. I also want to thank Professor Jos Vander Sloten for the valuable input given to this work and for the wise advices both during last year and this semester. To professor Maria Augusta Neto, for being my supervisor in Coimbra and for the confidence placed in me.

I must also thank Tristan Kuijpers for introducing me to the *Aladyn* project, and, of course, to Dennis Vandenbussche for providing me the opportunity to work in such an interesting project.

A huge thank you to Wouter Aerts, for being the best mentor any student could ask for. Thank you for all the patience, kindness, willingness to help and for repeatedly answering my questions. To Tiago Malaquias, for putting so much effort into this topic and for working side by side with me. Thank you for the motivation, enthusiasm and invaluable contribution. To Tassos Natsakis, for the valuable remarks and readiness to help whenever needed.

I feel very fortunate to have been part of such an exceptional team. I could not have asked for any better.

I cannot forget to thank professor Isabel Lopes for making possible my participation in both Erasmus and Erasmus+ mobility programs.

A big thank you to my friends in Coimbra and in Leuven, for being my constant inspiration, for reminding me of what is really important in life and for making this ride so wonderful.

Finally, I want to thank my beautiful family, for fully supporting and encouraging my adventures. For accompanying me, everyday, with no exception, even when living in a different country. Thank you for the endless support and for always believing in me.

Ana Carolina Pinto Silveira

Contents

Abstract

Current musculoskeletal foot-ankle models have a limited complexity and therefore they are not able to capture the full functionality of the foot-ankle complex. However, in the context of the *Aladyn* project, which aims at developing custom insoles with dynamic structures through 3D printing, there is need to model this complexity for extending the level of scientific evidenced-based insole design using multi-body dynamic simulations.

In this work, an extended musculoskeletal foot model is developed in OpenSim, incorporating the foot anatomical structures, intrinsic muscles and ligaments. A five-segment foot model is developed including a talus, calcaneus, midfoot, forefoot and toes segment. Five joints interconnect these segments and connect them with the lower leg segment: ankle (tibia-talus), subtalar (talus-calcaneus), chopart (calcaneus-midfoot), tarsometatarsal (midfoot-forefoot) and metatarsophalangeal (forefoot-toes). Two foot models were constructed with different number of degrees-of-freedom (DOF): an eight DOF and a fifteen DOF. Based on the number of foot segments spanned, thirty intrinsic muscles and thirty-six ligaments are included. The characteristic parameters of these anatomical structures are retrieved from literature. Experimental motion capture data, including marker trajectories, force and plantar pressure data of five healthy subjects is used to perform the scaling, inverse kinematics and inverse dynamics analysis.

Both the kinematic and dynamic results, are very consistent with literature. The eight DOF model proved to be more suitable to serve the purpose of this project. It presented less inter-subject variability when compared to the fifteen DOF model. The presence of ligaments in the model is found to contribute to the generation of joint moment and power. However, further work on the refinement of the parameters that characterize the intrinsic muscles and ligaments is necessary before proceeding to forward simulation analysis, and as such that it can be used in clinical practice.

Resumo

Actualmente, os modelos tridimensionais musculoesqueléticos do complexo pé-tornozelo não são representativos de toda a funcionalidade e complexidade do pé humano. Neste trabalho, inserido no projeto *Aladyn* (cujo objetivo é desenvolver palmilhas personalisadas com estruturas dinâmicas através da impressão 3D), há necessidade de criar um modelo mais representativo desta complexidade para elevar o nível científico do design de palmilhas através de simulações dinâmicas de corpos múltiplos.

Assim, é desenvolvido um modelo musculoesquelético do pé-tornozelo em *OpenSim*, incorporando estruturas anatómicas ao nível do pé: músculos intrínsecos e ligamentos. O modelo contém cinco segmentos: calcâneo, tálus, médio-pé, ante-pé e dedos. Os segmentos são interligados por quatro articulações: subtalar (tálus - calcâneo), chopart (calcâneo - médio-pé), tarsometatarsal (médio-pé - ante-pé) e metatarsofalangeana (ante-pé - dedos); e por sua vez, estes são ligados à parte inferior da perna através da articulação do tornozelo (tibia - tálus). Tendo em conta o número de articulações, são construídos dois modelos com diferentes graus de liberdade: um deles com oito e o outro com quinze graus de liberdade. De acordo com o número de segmentos do pé, são incluídos trinta músculos intrínsecos e trinta e seis ligamentos. Dados experimentais de captura de movimentos humanos *motion capture*, força e pressão plantar de 5 sujeitos saudáveis são usados para realizar o dimensionamento do modelo, bem como análises de cinemática inversa e dinâmica inversa.

Os resultados obtidos, tanto cinemáticos como cinéticos estão de acordo com a literatura. O modelo de oito graus de liberdade revela ser mais adequado para o propósito deste projeto, pois apresenta menos variabilidade inter-sujeito quando comparado com o modelo de 15 graus de liberdade. A incorporação de ligamentos no modelo demonstra contribuir para a geração de momento e energia, principalmente ao nível das articulações do médio-pé e ante-pé. É necessário trabalho futuro no sentido de ajustar os parâmetros que caracterizam os músculos e os ligamentos, antes de se avançar para aplicações em dinâmica direta, tal que o modelo possa ser utilizado em práticas clínicas.

List of Figures

List of Tables

List of Abbreviations and Symbols

Abbreviations

AB	Abduction
ABDH	Abductor Hallucis
ABDM	Abductor Digiti Minimi
AD	Adduction
ADHO	Adductor Hallucis Oblique
ADHT	Adductor Hallucis Transverse
a.-p.m.-t.	Anterior-posterior mid-tarsal axis
CT	Computer Tomography
d.a.	Dorsiflexion axis
DI	Dorsal Interosseous
DF	Dorsiflexion
DOF	Degrees of Freedom
EDB	Extensor Digitorum Brevis
EHB	Extensor Hallucis Brevis
EV	Eversion
FDB	Flexor Digitorum Brevis
FDMB	Flexor Digiti Minimi Brevis
FHB	Flexor Hallucis Brevis
FHBL	Flexor Hallucis Brevis Lateralis
FHBM	Flexor Hallucis Brevis Medialis
IC	Initial Contact
IMD	Inter-Marker Distance
IV	Inversion
LB	Lumbricals
MoCap	Motion Capture
o.m.-t.	oblique mid-tarsal axis
p.a.	plantarflexion ankle axis

PCSA	Physiological Cross-Sectional Area
PF	Plantarflexion
PI	Plantar Interosseous
QPL	Quadratus Plantar Lateralis
QPM	Quadratus Plantar Medialis
SD	Standard Deviation
t.c.n.	Talo-calcaneo-navicular axis
TO	Toe Off
XML	Extensible Markup Language
1r.	Fist ray axis
5r.	Fifth ray axis

Symbols

$C(q, \dot{q})$	Vector of Coriolis and centrifugal forces
F	Force
$G(q)$	Vector of gravitational forces
k	Stiffness
L_0	Ligament resting length
L	Ligament length
M	Moment of force
$M(q)$	System matrix
P	Power
q	Vector of generalized positions
$\dot{q}$	Vector of generalized velocities
$\ddot{q}$	Vector of generalized accelerations
ε	Strain
τ	Vector of generalized forces
ω	Angular velocity

Chapter 1

Introduction

Gait is the most common of human movements. Even though it is usually taken for granted, it is one of the most complex and totally integrated movements. It has been described and analysed more than any other movement. In fact, understanding the actual patterns of movement of humans and animals goes back to prehistoric times [1]. In 1836 the Weber brothers made one of the first mechanical analysis of human locomotion, describing the phases of human walking as well the motion of the centre of mass. They also analysed disorders of the gait pattern [2]. The appearance of photographic and motion picture cameras contributed to revolutionize the study of the human movement, revealing details that were not possible to visualize before. In 1887 Muybridge presented sequential photography techniques to analyse human gait [3], [2]. In the 19th century it was possible to perform the very first recordings of human locomotion patterns [1]. Nowadays it is possible to conduct even more precise experiments due to: the development of more accurate motion capture systems, which make use of video, infra-red cameras and laser or acoustic emission systems (e.g. Vicon ®, Oxford Metrics, UK); the use of force plates and plantar pressure measurement systems; furthermore, advances in the computer simulation field allowed estimating dynamic variables that cannot be directly observed or measured, for instance, the muscle forces or the trajectory of the bodies' centre of mass, moments of force, mechanical energy, etc. Consequently, musculoskeletal models, in which the human body is divided and modelled in segments that are interconnected by joints, have become a popular tool to study human gait as well as to calculate muscle forces in combination with dynamic simulations of motion, since they make use of inverse solutions to estimate or calculate these dynamic variables [2]. Thus, biomechanical modelling techniques can be used as a diagnostic, surgery planning or rehabilitation tool that can guide clinical decision making, or simply increase the quality of life of healthy subjects by providing more suitable footwear. This is possible thanks to the simulation and prediction tools, allowing to reveal, for instance, how much muscle strength is required to do a certain movement, or the forces and moments that a musculoskeletal system produces during a specific motion, or even to understand how changing the insertion point of a tendon can affect its moment curve profile.

However, in the current musculoskeletal models, the level of detail included to describe foot biomechanics is limited. Nevertheless, biomechanical modelling of the foot can, among others, actively contribute to: study gait disorders and pathologies related to the foot, improve athletic performance or design subject-specific customized insoles.

Therefore, this master thesis aims to develop an extended musculoskeletal model of the human foot in OpenSim, a freely available, user extensible software that allows the development of musculoskeletal models and dynamic simulations of movement [4].

1.1 Defining the Problem

The foot provides support to the human body by distributing gravitational and inertial loads [5]. Despite playing a fundamental role in human gait, there is still much to unveil before it is possible to fully understand its intrinsic kinematics and dynamics. It is a structurally complicated unit and its basic load-carrying mechanisms remain a vivid subject of debate in the biomechanics community [6]. So far, an unbiased understanding of the foot kinematics has been difficult to achieve due to, precisely, the complexity of the foot structure and motion [6]. This complexity arises from the number of small bones, muscles and ligaments that the foot is able to comprise. Due to this elaborateness, biomechanical models often treat the foot as a rigid segment, with no relative movement between the functional units or segments within the foot [7], [8]. Consequently, these models do not provide a realistic representation of the foot structure and its kinematics. As a result, the multi-segmental and deformable properties of the foot are not taken into account. While the use of these simple models might be reasonable to quantify ankle moments and powers during gait using inverse dynamics analysis [9], it is not advisable for performing contact simulation analysis or for modelling the effect of foot insoles on the movement of the foot structure. Furthermore, in many foot disorders (for example, flat feet, midfoot break, overpronation, etc.), these simple models do not allow a valid representation of the specific dysfunction that is often related to pathological movement between individual foot segments. In these cases, a realistic representation of the foot structure and its kinematics is required.

Multi-segment kinematic foot-ankle models, have been defined to capture foot kinematics and quantify it in health and disease [10]. They simplify the complex anatomical structure of the foot by grouping several neighbour bones together, creating the so called foot segments. The segments then act as rigid bodies, meaning that there is no movement within the segment. These kinematic models are primarily used for clinical gait analysis purposes, quantifying the joint angles and moments. They differ from musculoskeletal models as muscles are not included in kinematic models. As such, the aim of kinematic models is to analyse and document inter-segment motion.

For simulation purposes, the current musculoskeletal models should not only incorporate a similar multi-segment definition as the kinematics models. In addition,

the characteristic parameters of the foot muscles and ligaments, such as the ligament slack length, the muscle physiological cross sectional area or force, need to be defined. This specific information is currently only limited available as there are only very few studies concentrating on experimentally documenting these specific parameters.

In conclusion, the state of the art for musculoskeletal models of the foot-ankle complex for use in dynamic simulations of gait are highly simplified and do not account for the complex ligamentous and muscle control of the foot-ankle kinematics. The development of a detailed foot-ankle model is a pre-requisite to increase the understanding of foot pathologies and the design of adequate therapeutic interventions.

1.2 Objectives and Motivation

This master thesis is developed in the context of the *Aladyn* project, a joint collaboration between three industrial partners, Materialise NV, RS Scan and RS Print, and the KU Leuven as the research partner. The goal is to produce custom insoles with dynamic structures through 3D-printing. In order to do this, it is necessary to have a more scientific evidence-based insole design approach, since until now this process is mainly based on subjective decision making by the orthotic technicians, without a consistent and solid base. Thus, the *Aladyn* project aims at creating a fully automated digital workflow from patient assessment to the production of subject-specific insoles based on objective evidence. There are three distinctive knowledge domains identified in this project: biomechanical patient assessment, evidence-based insole design through modelling and 3D-printing of insoles with dynamic structures. This thesis work falls into the second knowledge domain.

Therefore, the primary purpose of this master thesis is to define and validate an extended foot-ankle musculoskeletal model in OpenSim. The specific objectives are:

- Increasing the level of detail of the current OpenSim foot model, by extending the anatomical and functional detail of the foot structures: firstly, the number of foot segments and the degrees-of-freedom (DOF) between them need to be increased to represent physiological foot function. This goal must be accomplished based on a literature study documenting in detail the foot-ankle kinematics and the associated joint axes. Secondly, the most relevant intrinsic muscles and ligaments of the foot that control the included segments need to be incorporated. This goal must be accomplished by investigating and gathering the respective muscle/ ligament parameters and geometry information from literature. The model definition will be implemented according to the OpenSim model formulation.

- Validation of the performance of two foot-ankle models, one with 8 DOF and the other with 15 DOF. This relies on inverse kinematics analysis using a data set of 3D integrated motion capture (MoCap) that included a multi-segment foot definition. Calculated kinematics are compared against a golden standard of foot-ankle kinematics obtained through bone anchored pins.

- Evaluation of the ligament forces by performing inverse dynamics analysis. Ranges of ligament forces are evaluated only qualitatively, as no golden standard is available in literature.

The expected outcome of this work is the development of an extended musculoskeletal foot model, that can be used, in combination with 3D motion capture and dynamic motion simulations, as a decisive tool in the making of customized 3D-printed insoles.

1.3 Document Structure

The second chapter of this thesis consists of the literature study. It starts by presenting the anatomy of the human foot, followed by the human gait cycle. The last section of the chapter focus on reviewing the already existing solutions regarding kinematic, kinetic and musculoskeletal models. Chapter 3 consists of the methods used to extend and validate the developed foot model. It defines the model construction procedure, as well as the scaling and validation. The fourth chapter presents the results obtained in terms of kinematics and dynamics. Chapter 5 discusses the results obtained as well as the challenges faced during the course of this work. At the end of each chapter a brief conclusion is presented, except for chapter 5, since its conclusion is part of the final chapter. Finally, in the last chapter, a conclusion is formulated and future work is defined.

Three appendices are included in this work. Appendixes A and B present the input parameters to model the intrinsic muscles and ligaments. Finally, appendix C includes the abstract of the publication to be presented in the thirteenth International Symposium on Computer Methods in Biomechanics and Biomedical Engineering 2015 (CMBBE), by the KU Leuven Ankle-Foot group.

Chapter 2

Literature Study

The aim of the present chapter is to address the anatomy of the foot in terms of its bones, joints, intrinsic muscles and ligaments, providing an overview of the important anatomical structures that need to be added to the extended musculoskeletal model of the foot. Secondly, the different phases of the human gait cycle are briefly explained. Finally, a literature review of the already existing kinematic and dynamic foot models is presented and a brief conclusion is formulated.

It is necessary to first establish the terminology used in this work in terms of the anatomical reference system, as a variety of terms that describe the 3-dimensional movement of the foot are found in literature. Figure 2.1 shows the reference planes with respect to the human anatomy. The sagittal plane divides de body into a right and a left part; the frontal, also known as coronal plane, divides the body into an anterior and a posterior part; and the transverse or horizontal plane is perpendicular to the sagittal and frontal planes. Therefore, the vertical axis is the Y axis, the anterior-posterior direction is the X axis and the medial-lateral direction is the Z axis, figure 2.1. Furthermore, the terminology used in this work to describe the 3D movement of the foot is as follows: dorsiflexion/plantarflexion or extension/flexion correspond to rotation about a medial-lateral axis; abduction/adduction, to rotation about a vertical axis; and inversion/eversion to rotation about an anterior-posterior axis. It is also important to note that some authors, such as Hicks [11], refer to the rotation about an anterior-posterior axis as supination/pronation whilst in this work this rotation is referred to as inversion/eversion. The terminology supination/pronation is used in this work to describe a combined movement of inversion/eversion in the frontal plane, adduction/abduction in the transverse plane and plantarflexion/dorsiflexion in the sagittal plane, respectively.

2.1 Anatomy of the Human Foot

The human foot is considered to be a very complex and intricate structure due to the number of elements and joints it comprises despite its relatively small size. It is, therefore, essential to understand the basics of the foot anatomy in terms of bones, joints, muscles and ligaments, as well as understanding the interaction between these

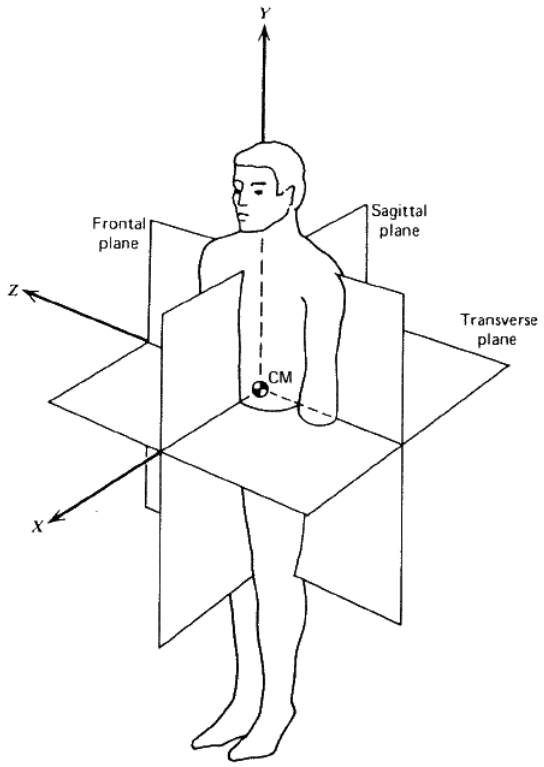

Figure 2.1: Reference planes with respect to human anatomy. Figure adapted from [12]

structures in order to build a biomechanical foot model. *Regardless of what research defines as the human gait cycle and the role of the foot, the one constant remains anatomy* [13], being of paramount importance to understand it before anything else.

2.1.1 Foot Bones

The foot includes twenty-six bones: seven tarsals, five metatarsals and fourteen phalanges, figure 2.2. The tarsals are the talus, calcaneus, navicular, three cuneiforms (medial, intermediate and lateral) and the cuboid. The arrangement and relative positioning of the bones imposes a limited independence between them [13].

The talus plays the critical role of connecting the lower leg to the foot since it articulates with the tibia and fibula, which are the lower leg bones, and it also articulates with the calcaneus and navicular. The calcaneus is the largest bone of the foot and is commonly referred to as the heel bone. It contains three articular surfaces (the posterior, middle, and anterior facets) allowing the talus to articulate with it, forming the subtalar joint. The navicular is located between the head of the talus and the three cuneiforms and it has a flattened oval shape. It connects with the talus through the talonavicular joint. The three cuneiforms are all wedge shaped and line up side by side in the midfoot, with the broader side of the wedge oriented

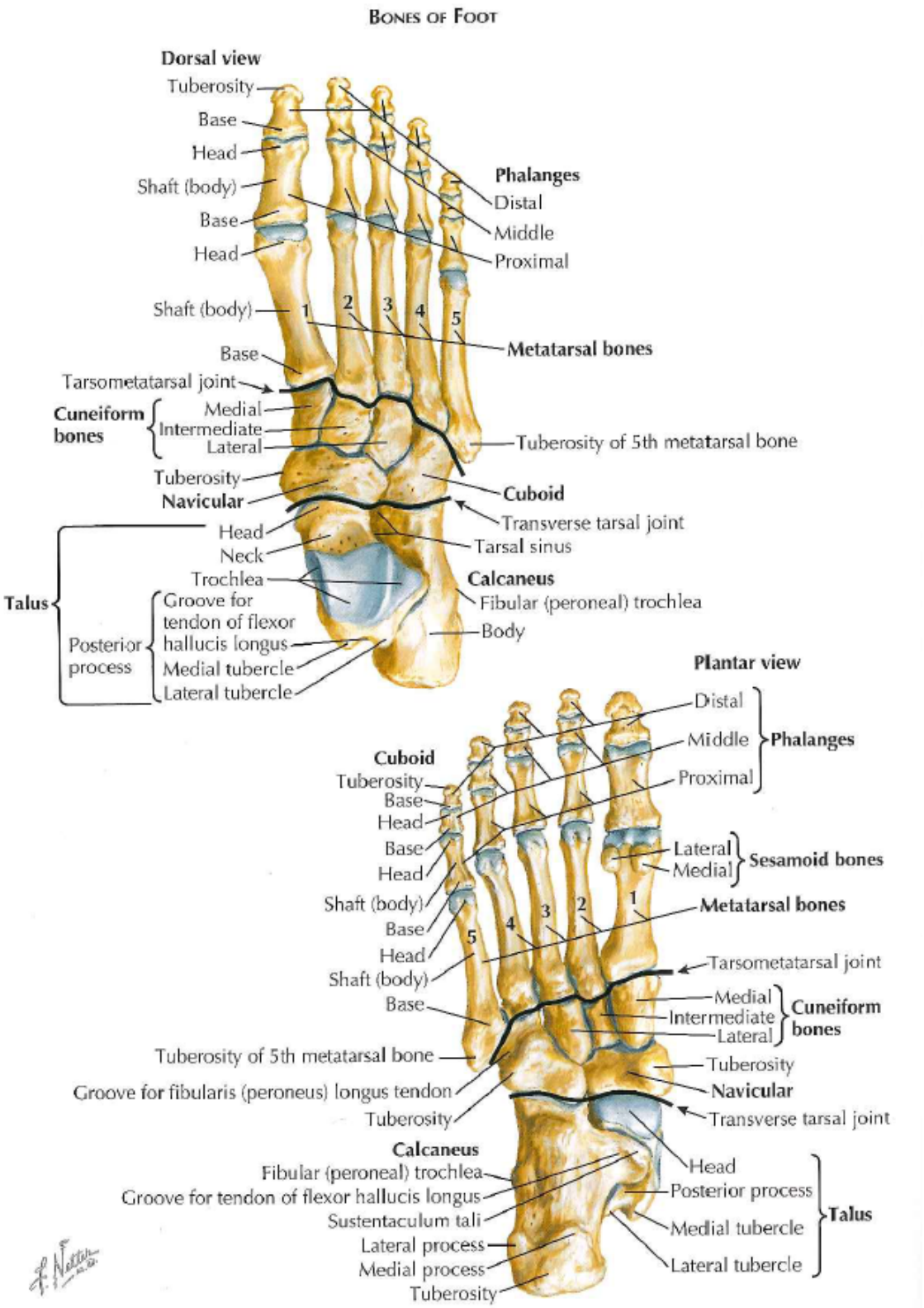

Figure 2.2: Bones of the foot, dorsal and plantar view. Figure adapted from [13]

plantarly on the medial cuneiform and dorsally on the intermediate and lateral cuneiforms. They articulate with the navicular forming the naviculocuneiform joint. The cuboid is a square-shaped bone on the lateral side of the foot interposed between the calcaneus and the fourth and fifth metatarsals. The main joint formed with the cuboid is the calcaneocuboid joint. The metatarsals are long bones, relatively flat dorsally and concave longitudinally on the plantar sides. They are each composed of a base, a body and a head and are numbered from one (medial) to five (lateral). The bases of the second and third metatarsals articulate with the cuneiforms and the base of the fifth with the cuboid, creating the Lisfranc joint (or the tarsaometatarsal joint). The heads articulate with the proximal phalanges, forming the metatarsophalangeal joint. The first metatarsal is the broadest and most massive of the five. It has a broad head and its plantar surface has two grooves where the sesamoids lie within the tendons of the flexor hallucis brevis muscle. Finally, the phalanges are the bones of the toes. They are short and are divided into proximal, middle and distal. Each toe has three bones except for the great toe which has two [13].

2.1.2 Foot Joints

A joint is defined as the place where two bones connect or articulate. In terms of joint function, there are three different joint classes: the synarthroses, which are immovable since the surfaces of the bones are in almost direct contact; the amphiarthroses, which are slightly movable, being the surface of the bones connected by ligaments or cartilage; and the synovial joints or diarthroses, which are the most common in the human body. The latter are characterized as freely movable joints, in which there is space between the adjoining articular surfaces and the space is lubricated by synovial fluid. The synovial joints are the most relevant as all the joints studied in this work are of the synovial type. These joints can be classified in several types according to the kind of motion permitted in each of them. The following synovial joints are present in the foot: the Hinge joint, where motion is only possible in one plane, for example, the interphalangeal joint; the Gliding joint, also known as planar joint, admits a gliding movement in any direction along the plane of the joint, it can be found between bones that have flat articular surfaces, being the tarsometatarsal joint an example; and the Condyloid joint, in which flexion, extension, adduction, abduction and circumduction are possible and it is present, for example, in the metatarsophalangeal joint [14].

Ankle Joint

The ankle joint is the articulation between the tibia and the talus and it is agreed to be a synovial joint of the hinge type, also known as tibiotalar joint. The synovial membrane of the ankle joint has the capacity to extend upwards, causing large amount of synovial liquid to concentrate there [13]. The primary movement of this joint is dorsiflexion (extension) and plantarflexion (flexion), however just like in most of the foot joints, there is a combination of other minimal movements happening at the joint as opposed to a unique and simply defined movement. As described by

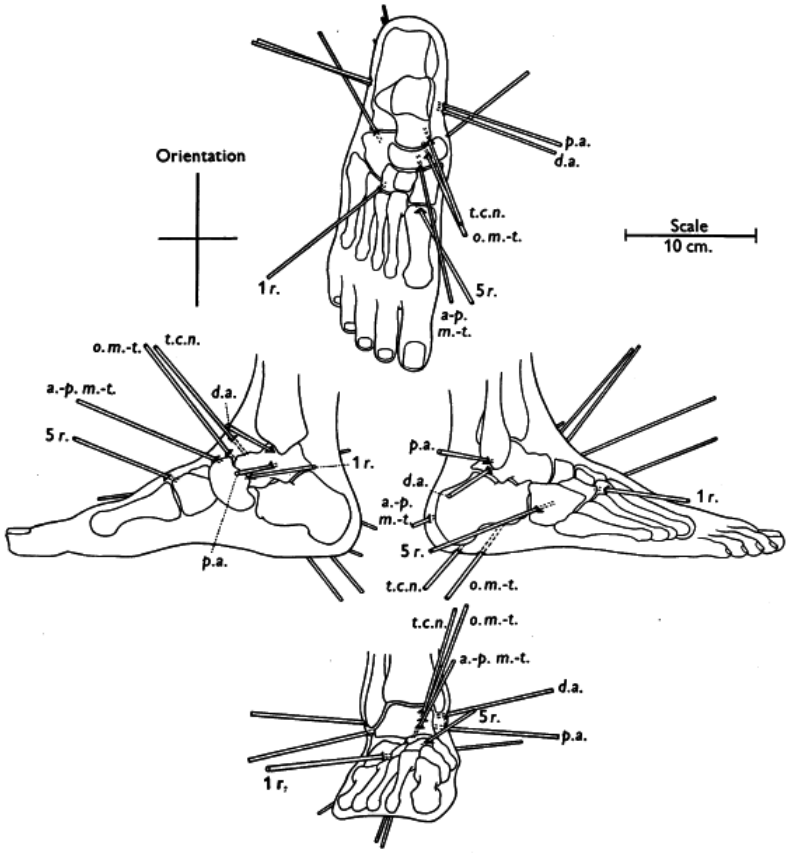

Figure 2.3: Schematic representation of the foot axis defined by Hicks [11]: the plantarflexion ankle axis (p.a.), dorsiflexion ankle axis (d.a.), talo-calcaneo-navicular axis (t.c.n.), oblique mid-tarsal axis (o.m.-t.), anterior-posterior mid-tarsal axis (a.-p. m.-t.), first ray axis (1r.) and fifth ray axis (5r.). Figure adapted from [11]

Hicks [11] and in agreement with the work of Barnett and Napier [15], a dorsiflexion ankle axis (d.a.) and plantarflexion ankle axis (p.a.) were defined at the ankle level, 2.3. These axis are oblique in both the sagital and transverse planes, therefore, the minor and minimal movements that accompany flexion-extension at the ankle are abduction/adduction and inversion/eversion [16].

Subtalar and Talocalcaneonavicular joints

The subtalar joint is one of the six intertarsal joints, being the other five the talocalcaneonavicular, calcaneocuboid, transverse tarsal, cuneonavicular and intercuneiform. It is the joint between the underside of the body of the talus and the posterior surface of the superior aspect of the calcaneus. There is a loose, thin-walled articular capsule uniting the bones in the margins of the articular surfaces [13].

The talocalcaneonavicular joint is composed of two joints that function as a unit: the posterior talocalcaneal joint and the anterior talocalcaneal joint. The axis of this

joint, according to [11] is oblique, oriented upward, anteriorly and medially and has a transverse, vertical and longitudinal component. Each component generates motion, hence, this joint produces a combination of three motions: eversion-abduction-extension or inversion-adduction-flexion.

Chopart Joint

The transverse tarsal joint, also known as Chopart joint, crosses the foot from side to side, consisting of the talonavicular and the calcaneocuboid joints [13]. The talonavicular joint is an integral part of the talocalcaneonavicular complex and moves along with the subtalar joint but it can also move in unison with the calcaneocuboid joint, independently of the subtalar. Thus, the navicular rotates with respect to the talus about three different axis depending on which complex it is moving along with, but always acts as a hinge joint. The calcanocuboid is a saddle joint [16].

As presented in figure 2.3, and according to Hicks [11] there are two axis that define the Chopart joint: the oblique mid-tarsal axis (o.m.-t.) and the anterior-posterior mid-tarsal axis (a.-p. m.-t.). The movement allowed in the first one is eversion-abduction-extension or inversion-adduction-flexion and in the latter eversion with slight abduction-extension or inversion with slight adduction-flexion. In conclusion, these joints contribute mainly to the inversion/ eversion of the foot.

Tarsometatarsal Joint

The tarsometatarsal, also known as Lisfranc's joint, is composed of plane joints between the medial three metatarsals bases with the cuneiforms, and the two lateral metatarsals bases with the cuboid. It allows flexion/extension of the metatarsal rays and some longitudinal axial rotation-inversion and rotation-eversion at the marginal rays [16]. Observing figure 2.3, it is possible to identify two axes at the tarsometatarsal joint: the 1st ray axis (1 r.) and the 5th ray axis (5 r.). Both axes allow for flexion-eversion or extension-inversion [11].

Metatarsophalangeal Joint

These joints are condyloid joints between the heads of the metatarsals and the extremities of the proximal phalanges. As such, dorsiflexion, plantarflexion, abduction, adduction and circumduction are the movements at these joints. However, the primary movement is, undoubtedly, dorsiflexion/plantarflexion. Each joint is enclosed by an articular capsule and reinforced by plantar and collateral ligaments [13].

2.1.3 Intrinsic Muscles

The muscles are the structures that allow bone movements through its contractile forces. As agglomerates of fibers, they are responsible for creating movement in the human body. The sarcomere is the functional unit of the muscles, and it is composed of contractile proteins or filaments which are the responsible for the muscle contraction. A muscle contracts when it is activated and this activation is controlled

by the somatic nervous system, which triggers an action potential. When contracting, the muscles develop force and create a torque about one or more joints spanned by those muscles. Nevertheless, muscles are able to accelerate bodies that they do not span due to a phenomenon denominated dynamic coupling, in which *a force applied by each muscle is transmitted through the bones of the skeleton to all the joints* [17].

The tendons, which are strong fibrous collagen tissue, attach the muscles to the bones of the skeleton. At the foot, extrinsic and intrinsic muscles are discriminated. The foot extrinsic muscles originate in the femur, tibia or fibula and insert on one of the foot bones, while the intrinsic muscles have both their origin and insertion points in the foot.

The intrinsic muscles of the foot are twenty-eight and are located both in the plantar and the dorsal aspects of the foot. It is widely accepted [13] [16] that the plantar foot can be divided in four relevant compartments: medial, lateral, central and interosseous.

The medial compartment comprises the abductor hallucis (ABDH) and flexor hallucis brevis (FHB) muscles as well as the tendon of the flexor hallucis longus (the last one is not considered an intrinsic muscle). The flexor hallucis brevis is a two-bellied muscle, divided into a medial and lateral component and it allows for the flexion of the hallux through the metatarsophalangeal joint. The abductor hallucis muscle, arising from the calcaneus and inserting into the base of the proximal phalanx of the big toe is the responsible for abduction of the great toe from the axis of the second ray.

The lateral compartment consists of the flexor digiti minimi brevis (FDMB) and abductor digiti minimi (ABDM). The first flexes the fifth toe through the metatarsophalangeal joint and the latter abducts the fifth toe from the axis of the second ray.

The central compartment contains the flexor digitorum brevis muscles (FDB), the tendon of the flexor hallucis longus and lumbricals (LB), the adductor hallucis and the quadratus plantae muscles. The flexor digitorum brevis muscles divides into four tendons and each one of them is then divided, in the proximal phalanges, into two splits that insert in the middle phalanges, figure 2.4. Thus, these muscles are responsible for flexion of the middle phalanges of the lateral four toes and also contribute to the metatarsophalangeal flexion of these toes. The quadratus plantar is divided into a medial and a lateral component (QPM and QPL) that merge to form a flattened muscular band. This muscle assists the flexor digitorum longus in flexing the toes. The lumbricals are four small cylindrical muscles that arise from the four tendons of the flexor digitorum longus and these muscles flex the proximal phalanges (at the metatarsophalangeal joint) and extend the middle and distal phalanges. The last muscles of the central compartment are the transverse and the oblique adductor hallucis (ADHT and ADHO). These muscles adduct the great toe and play an important role in maintaining the transverse arch of the foot [13].

Finally, the interosseous compartment comprises the plantar interosseous (PI) and the dorsal interosseous (DI). The first are adductors of the third, fourth and fifth digits while the second are abductors of the digits. Both of the interosseous serve in flexion of the metatarsophalangeal joints [13]. Figure 2.5 illustrates the origin and

insertion points of the intrinsic muscles of the foot.

Regarding the dorsal aspect of the foot, it includes the extensor hallucis brevis (EHB) and three extensor digitorum brevis muscles (EDB). Figure 2.4 shows the intrinsic muscles of the foot. The extensor digitorum brevis is a broad but thin muscle that divides into four tendons for the most medial four toes. However, the most medial tendon, which is the largest of the four, is often designated as extensor hallucis brevis muscle [13] [18], as it is possible to observe in figure 2.4. The other three tendons merge with the tendons of the extensor digitorum longus (which is not an intrinsic muscle) in the second, third and forth toes, assisting in the extension of the proximal phalanges [13].

2.1.4 Ligaments

Ligaments are strong structures that attach bones to other bones. They are composed of flexible, fibrous connective tissue and are responsible for stabilizing the joints. Even though they are flexible, they are also rather stiff structures in which small length changes can cause large passive forces. A brief overview of the ankle-foot ligaments that are the most relevant to this work is presented. Figure 2.6 illustrates the ligaments of the ankle-foot complex.

Ankle Ligaments

The ligaments responsible for stabilizing the ankle joint can be divided into three groups depending on their anatomical location: the lateral ligaments, the deltoid ligaments on the medial side, and the ligaments of the tibiofibular syndemosis [19]. The first two groups are composed of notably strong ligaments.

The lateral collateral ligament complex consists of the anterior talofibular, the calcaneofibular and the posterior talofibular ligaments. Firstly, the anterior talofibular ligament limits the anterior displacement of the talus and plantarflexion of the ankle. It is virtually horizontal to the ankle in neutral position but inclines upward in dorsiflexion and downward in plantarflexion. Only in plantarflexion the ligament comes under strain. Secondly, the calcaneofibular is the only ligament bridging both the talocrural and subtalar joint. It allows flexion/extension of the talocrural joint and also permits subtalar movement depending on its bi-articular characteristics. The calcaneofibular becomes horizontal during plantarflexion and vertical in dorsal flexion, remaining tensed throughout the entire arc of motion of the ankle and is relaxed while everted and tense during inversion. Thirdly, the posterior talofibular ligament is relaxed in plantarflexion and in neutral ankle position, while in dorsiflexion it is tensed. Since it is a multifascicular ligament, it does not insert in a specific unique place and some of its fibers contribute to form the tunnel for the flexor hallucis longus tendon while other fibers fuse with the posterior intermalleolar ligament [19], [16].

The medial collateral ligament, also known as the deltoid ligament, is a strong and triangular multifascicular group of ligaments and can be divided into a superficial and deep group of fibers. It originates from the medial malleolus to insert in the talus,

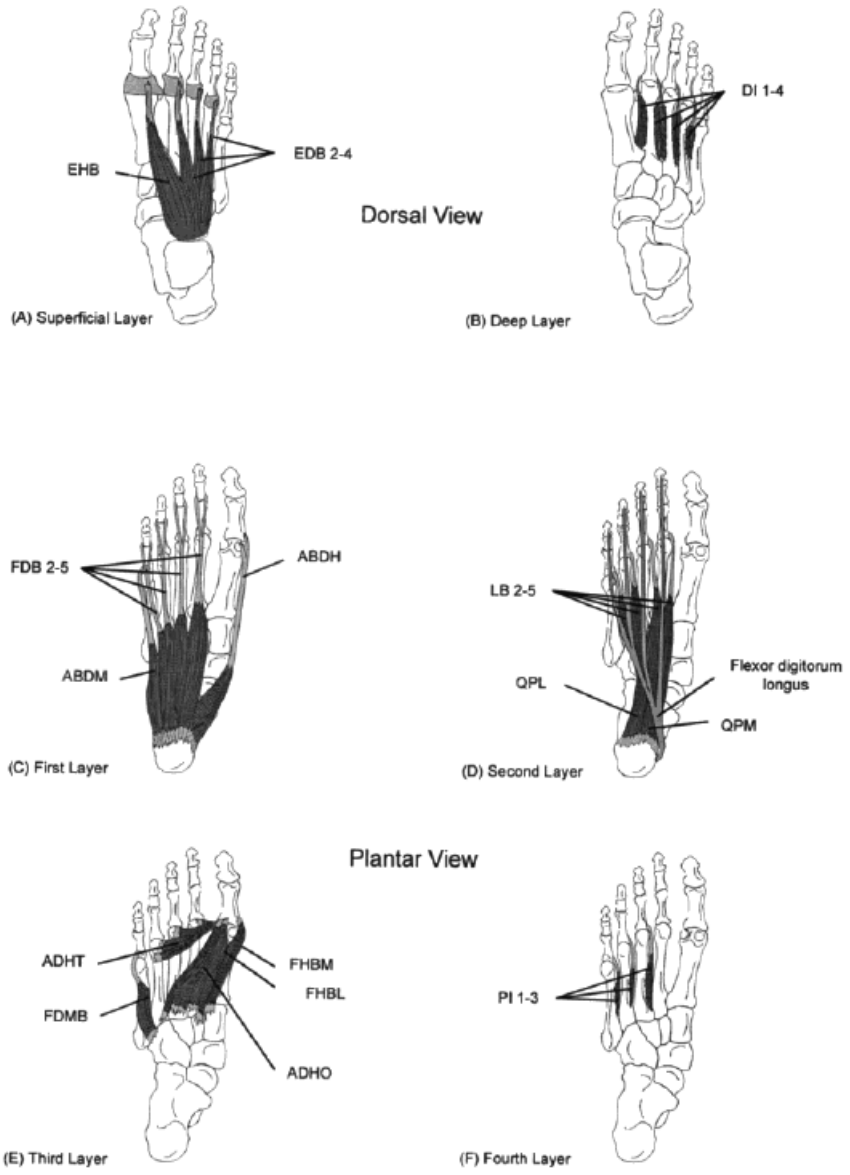

Figure 2.4: The dorsal and plantar views of the intrinsic muscles of the foot. The nomenclature is abbreviated in the figure: m. extensor hallucis brevis (EHB), three mm. extensor digitorum brevis (EDB 2-4), four mm. dorsal interosseous (DI 1-4), four mm. flexor digitorum brevis (FDB 2-5), m. abductor digiti minimi (ABDM), m. abductor hallucis, four mm. lumbricals (LB 2-5), mm. quadratus plantar medialis (QPM) and lateralis (QPL), m. adductor hallucis transverse (ADHT) and oblique (ADHO), mm. flexor hallucis brevis medialis (FHBM) and lateralis (FHBL), m. flexor digiti minimi brevis (FDMB) and three mm. plantar interossei (PI 1-4). Figure adapted from [18]

.

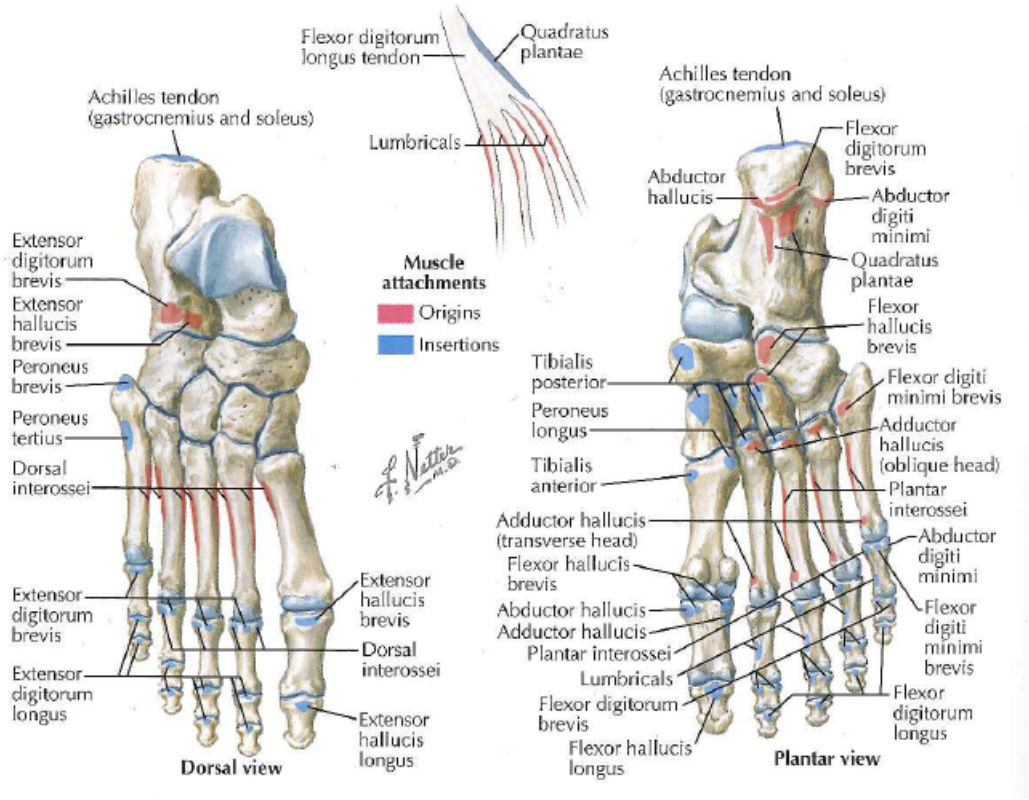

Figure 2.5: Origin and insertion points of the intrinsic muscles of the foot: dorsal and plantar view. Figure adapted from [13]

calcaneus and navicular. Even though there is not much agreement in literature, the most commonly accepted description of this ligament is that it comprises six bands: three that are always present, the tibiospring, the tibionavicular and the deep posterior tibiotalar ligament, which is the thickest [13] and strongest component of the entire medial ligament [16]; and the other three that can vary, the superficial posterior tibiotalar ligament, tibiocalcaneal ligament and deep anterior tibiotalar ligament [19].

The tibiofibular syndesmotic ligament complex ensures the stability of the tibia and fibula and resists the axial, rotational and translational forces that attempt to separate them. The three ligaments responsible for this are the anterior tibiofibular, the posterior tibiofibular and the interosseous tibiofibular ligament.

Talocalcaneonavicular Ligaments

The talocalcaneonavicular complex comprises the inferior, lateral, posterior, medial, superomedial and interosseous calcaneonavicular ligaments. The inferior calcaneonavicular ligament, also known as the spring ligament due to its elasticity, is very fasciculated consisting of a thick bundle of fibers, being the lateral bundle (that inserts on the beak of the navicular), the strongest. The lateral calcaneonavicular

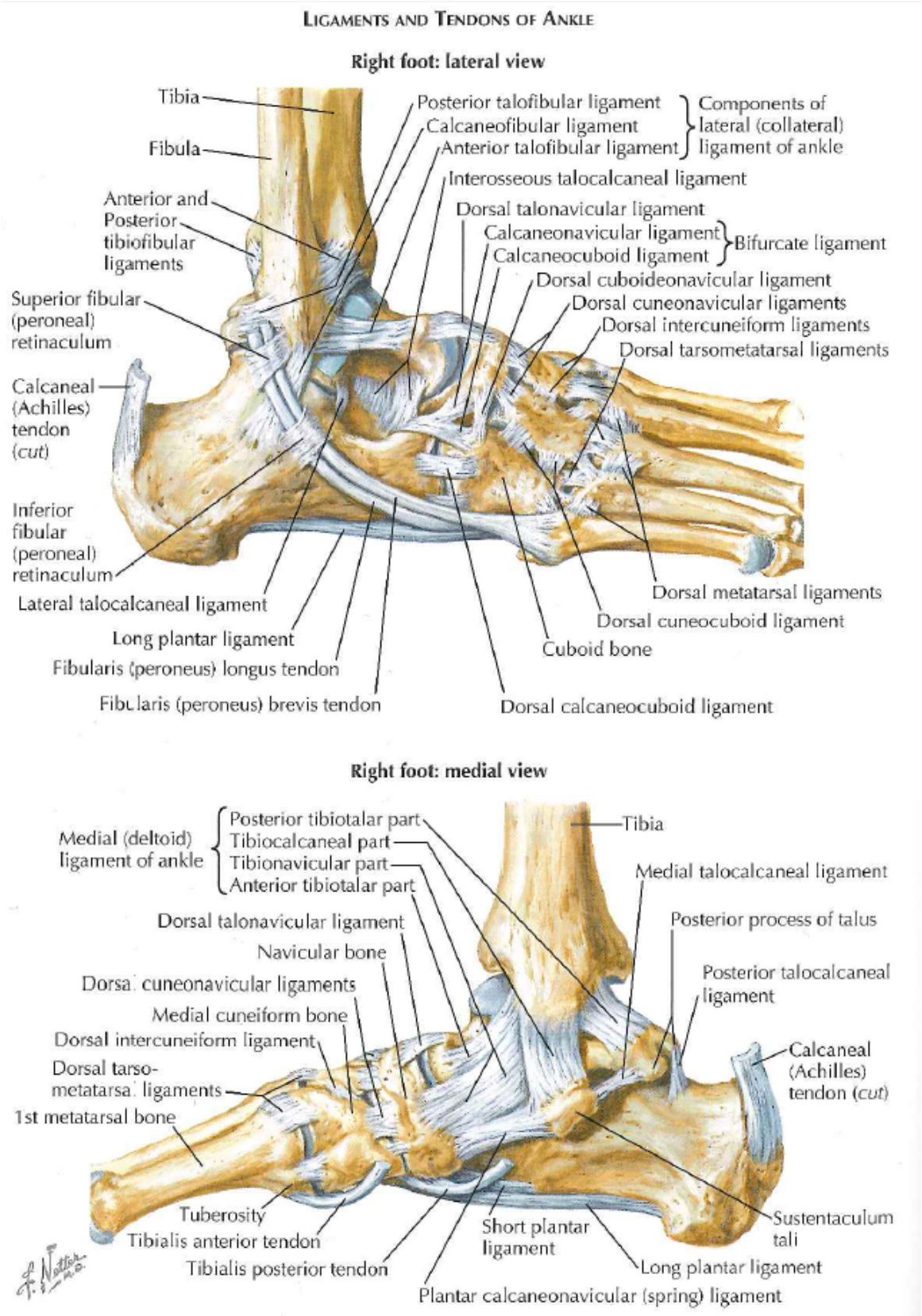

Figure 2.6: Ligaments and tendons of the ankle-foot complex: medial and lateral view. Figure adapted from [13]

is part of the bifucarte ligament, which is disposed in the form of a V forming an average angle of 30 degrees between the two components. The other component of the bifurcate ligament is the medial calcaneocuboid and it is usually the least strong component of the V-shaped ligament. Besides the ones mentioned above, the talocalcaneonavicular joint also includes the cervical ligament (it is a part of the interosseous ligament and is also called anterior talocalcaneal ligament) which is the strongest ligament connecting the talus and the calcaneus. Finally, there is the talonavicular ligament, which has a superficial and a deep component, being the first a thin, long band and the second a shorter but deeper band [16].

Hindfoot-Midfoot Ligaments

There are numerous ligaments connecting the hindfoot bones to those of the midfoot, as well as interconnecting the tarsal bones. At the calcaneocuboid joint, three ligaments are identified: the medial, dorsolateral and inferior calcaneocuboid ligaments. The medial ligament is the outer component of the bifurcate ligament, as mentioned above. The inferior calcaneocuboid is a thick, powerful plantar ligament with a deep and a superficial component: the short plantar and the long plantar ligaments.

Each of the three cuneiform bones is united to the navicular by both a dorsal and a plantar ligament. The cubonavicular, the dorsal cuneonavicular and the cuneo-cuboid ligaments each have three types: a dorsal, plantar and a interosseous.

Lastly, there are two dorsal, two interosseous and one plantar intercuneiform ligaments to keep these three bones together. The dorsal are small rectangular bands, the plantar is a short ligament, while the interosseous is a strong thick transverse ligament [16].

Tarsometatarsal Ligaments

The tarsometatarsal joint is very complex one and is secured by seven dorsal ligaments, by a variable number of plantar ligaments and by three sets of interosseous ligaments. The dorsal ligaments guarantee the connection between the bases of the first three metatarsal rays and the three cuneiforms and between the fifth metatarsal and the cuboid. Even though the plantar cuneometatarsal ligaments are always present, its number and location vary from subject to subject. These ligaments are, in general, stronger than the dorsal ones. The interosseous ligaments are located in the interspace between the three first metatarsals and the cuneiforms, being the first one the strongest of the three (also known as the Lisfranc ligament). Finally, there are the intermetatarsal ligaments in between the metatarsals, and they can also be characterized in dorsal, plantar and interosseous. It is noteworthy to mention that there is no dorsal or plantar ligaments between the first and second metatarsals [16].

Metatarsophalangeal

In the metatarsophalangeal joint, the proximal phalanx and the fibrocartilaginous plantar plate constitute both an anatomical and functional unit. It is at the plantar plate that the two longitudinal septae of the plantar aponeurosis insert as well as

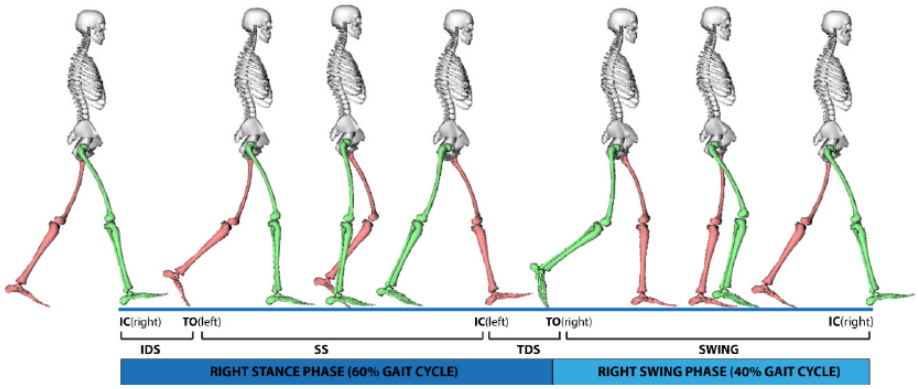

Figure 2.7: The human gait cycle: stance and swing phase of the right foot. During the stance phase (60% of the cycle) the foot is in contact with the ground, starting from initial contact (IC). The swing phase (40% of the cycle) starts from toe off (TO) and ends at initial contact (IC). Figure adapted from [20].

many tendons. The plantar plate is connected on its sides by the deep transverse intermetatarsal ligament. Also, the metatarsoglenoid suspensory ligament and the transverse lamina of the extensor aponeurosis insert on the dorsal side of the plantar plate [16].

Finally, the plantar ligaments of the foot are stronger and more extensive than the dorsal and their support function is enhanced by robust interosseous ligaments, since it is necessary to balance the foot against the weight of the body [13].

2.2 The Human Gait Cycle

The human gait cycle is divided in two distinctive phases: the stance phase, which comprises approximately 60% of the gait cycle; and the swing phase, comprising the remaining 40% of the cycle. One gait cycle consists of the period between two consecutive heel strikes of the same foot, figure 2.7.

The stance phase is initialized with the heel strike when the heel cushion makes contact with the ground. As the foot descends rapidly, the lateral part will then touch the ground. As the forefoot is in a supination position, the tibia rotates internally and the subtalar and chopart joints evert. The combination of eversion of the hindfoot and midfoot with the supination of the forefoot transforms the foot into a rigid structure. To reach the foot flat phase, which occurs at 15% of the gait cycle, the medial part of the foot progressively contacts with the ground. At this point, the ankle is in dorsiflexion, the hindfoot and midfoot invert and the forefoot is pronated. This combination will make the foot a more flexible bony structure, and, at this point the metatarsophalangeal joint of the great toe will be in neutral position. As the foot reaches the heel rise phase at 30% of the cycle, the forward momentum of the leg continues. The hindfoot and midfoot invert and the forefoot

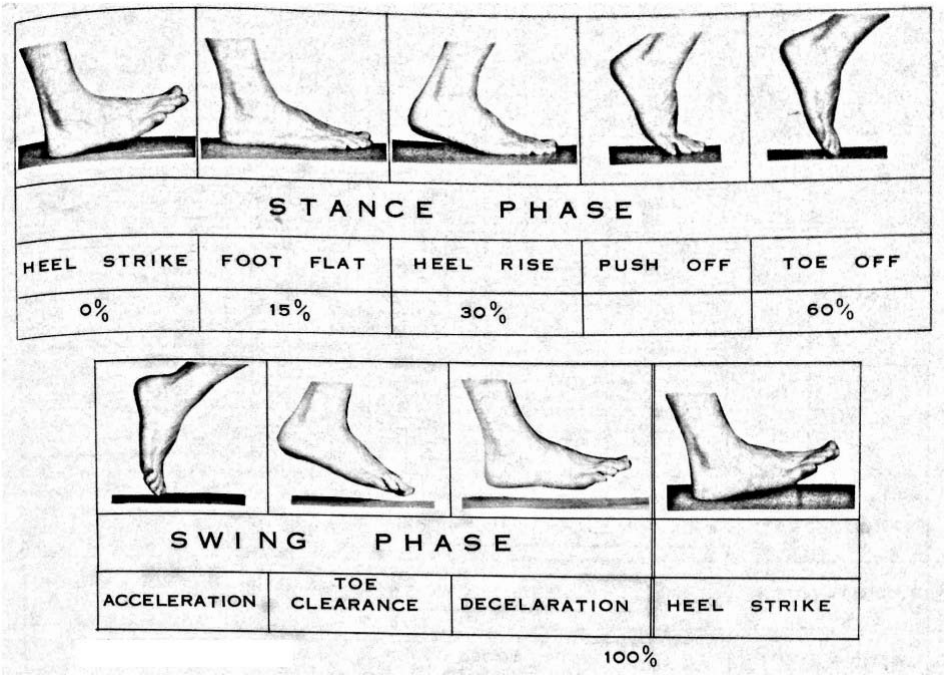

Figure 2.8: Detail of the stance and swing phase of the gait cycle. Figure adapted from [16]

increases the pronation position and the foot will acquire a loose status. However, as the foot progresses to the push off phase, it acts as a lever arm and maintains its rigidity. The plantarflexion continues at the ankle and the metatarsophalangeal joint of the great toe will reach its maximum of dorsiflexion around 45%-50% of the cycle, after which it will decrease until reaching again the neutral position. Finally, the toe off phase occurs at 60% of the gait cycle when the great toe breaks contact with the ground, starting the swing phase [16].

The swing phase corresponds to the period in which the foot is off the ground. At the beginning of this phase, the foot is accelerated and plantarflexed, then it gradually moves to dorsiflexion and eversion. In the last part of this phase, the foot is decelerated, the leg rotates internally and the heel inverts. To complete the cycle, the foot progressively descends to reach the ground and when it does, the ankle is in a 90 degrees position and the heel is minimally inverted [16].

2.3 State of the Art: Existing Foot-ankle models

Throughout the years, many foot models have been developed, differing in the number and the definition of its segments. The foot models serve distinctive purposes, thus, depending on its intent, the models can be used to perform different types of analysis, such as kinematic, kinetic, forward simulation, etc. Hence, depending on the purpose, kinematic, kinetic or musculoskeletal models can be developed. This section provides

an overview of the state of the art regarding some of the different types of foot models.

2.3.1 Kinematic and Kinetic Foot Models

Kinematics is defined to be the study of motion without considering the forces and moments that produce that motion. Kinematics, include linear and angular displacements, velocities and accelerations [1]. On the other hand, kinetics is defined to be the general term given to forces that cause movement. These forces can be internal, including muscle activity, ligaments, and force caused by friction in the joints; or external, such as the ground reaction forces and the external loads [1]. Thus, kinetics provide insight of the mechanics involved and of the strategies and compensations of the neural system. As stated by Winter [1], *a large part of the future of biomechanics lies in kinetic analyses, because the information present permits us to make very definitive assessments and interpretations.* In this sense, in order to develop kinetic (or dynamic) foot models, a set of requirements must be fulfilled: firstly, for every foot segment, the mass, centre of mass and moment of inertia need to be defined; additionally, it is necessary to know the external forces acting on each segment separately.

Most of the kinematic foot models described in literature divide the foot in three segments. The Oxford Foot Model [21] is one of them, presenting a multi-segment approach to measure foot kinematics during gait that was tested for its repeatability in healthy feet. The three segments are the hindfoot (comprising the calcaneus and talus), forefoot (metatarsals) and hallux (toes), allowing six degrees of freedom between any pair of segments. The inter-segment angular motion was examined in the three anatomical planes and consistent patterns and ranges of motion were detected. This model was used by Stebbins [8] where it was adapted to study children's feet. Another three segment foot model by Okita [10] divides the foot in shank (tibia and fibula), hindfoot (calcaneus and talus) and forefoot (tarsal bones, metatarsals and toes). In this publication the authors investigate the rigid body assumption and whether there are differences in the kinematics data from skin mounted markers and bone mounted markers. It was concluded that the shank and hindfoot behaved as rigid bodies while the forefoot violated the rigid body assumption since there was evidence of significant differences between motions of the first metatarsal and the forefoot as well as relative motion between the first and fifth metatarsals. In 1998, Rattanaprasert [22] also presented a three foot segment with a hindfoot, forefoot and hallux (in addition to a rigid leg segment) to study the effects of reduced functional activity of the tibialis posterior muscle on the motion of the foot. The motion differences observed in the study were consistent with the expected mechanical consequences.

Even though the previous models satisfied the goals they were meant for, it has been reported by Cobb [23] that significant movement occurs between the navicular and the first ray and that the medial and lateral forefoot function somewhat independently. The latter study investigated the effect of foot posture on gait kinematics using a four-segment foot model presenting four functional articulations:

hindfoot, calcaneonavicular complex, medial forefoot and first metatarsophalangeal complex. Sawacha [24] also developed a multi-segment foot model including the midfoot, since it was considered a limitation of literature not to evaluate the midfoot motion when characterizing the foot kinematics of diabetic patients. A five-segment foot model was established by Tome [25], consisting of tibia, hindfoot, medial forefoot, lateral forefoot and hallux segments. The medial forefoot was defined by the first metatarsal and the lateral forefoot including the second through fourth metatarsals. The goal of the model was to compare the stance kinematics of patients suffering from posterior tibialis tendon dysfunction to healthy subjects. Another five-segment foot model is presented by Leardini [26], including the shank, calcaneus, midfoot, metatarsals and hallux to study the motion during the stance phase of gait. Caravaggi [27] used this model to investigate the relationship between foot joints mobility and plantar pressure. The study states that pressure distribution can be seen as the effectiveness of the musculoskeletal system in absorbing the ground reaction forces via the foot and its joints. From the study it was noticed that the mean and peak pressure at the hindfoot and forefoot were negatively correlated with the amount of motion at the ankle and tarso-metatarsal joints. On the other hand, the pressure at the hallux and midfoot were positively correlated with the range of motion of the joints across the midfoot.

In 2002, MacWilliams [7] presented a model with a higher level of detail, incorporating nine segments to study the kinematics and kinetics during adolescent gait. As this model allows to study foot kinetics, it falls into both the categories of kinematic and kinetic models. The included segments are the hallux, medial toes, lateral toes, medial forefoot, lateral forefoot, calcaneus, cuboid, talus/navicular/cuneiform and tibia/fibula. Joint angles, moments and powers were calculated for eight articulations of the nine segments. The results indicated the complexity of gait, with specific foot joints generating power and others absorbing it. For instance, the results showed that while the tarsometatarsal joint generates power, the metatarsophalangeal absorbs a similar amount of power, therefore balancing the forefoot. Furthermore, the medial rays were found to carry higher loads, flex more and generate more power than the lateral rays, which is consistent with the fact of the first ray being structurally the largest. Using these more detailed foot models, it was possible to have a better understanding of ankle-foot kinematics and kinetics during gait. Mahaffey [28], evaluated three different foot models in terms of their repeatability in paediatric foot motion during gait: the Oxford foot model (by Carson [21]), the 3DFoot model (by Leardini [26]) and the Kinfoot model (by MacWilliams [7]). They concluded that the Oxford Foot Model showed moderate repeatability and reasonable errors except for the hindfoot; the Kinfoot provided abundant information on the foot kinematics but the errors were considered unacceptable; the 3DFoot model was found to offer an acceptable balance between repeatability and the kinematic information provided.

In 1993, Scott and Winter [29] proposed an eight-segment foot model interconnected by hinge joints to estimate joint kinematics and kinetics during the stance phase of the gait cycle. The plantar soft tissue of the foot was modelled as a set of springs and dampers in parallel. The structure of the model was based on the anatomy of the foot, figure 2.9. The results obtained from the kinematic and kinetic

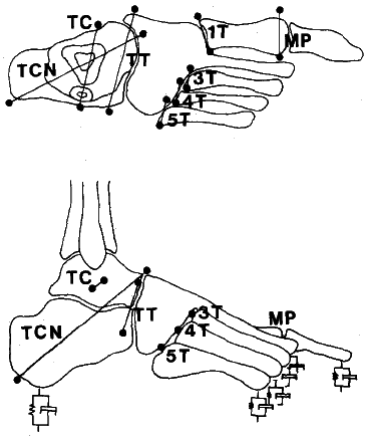

Figure 2.9: Eight segments of the human foot model proposed by Scott and Winter, 1993. Figure adapted from [29]

.

analysis allowed to classify the model as an objective tool able to quantify the motion and loading during the stance phase of walking, even though it was ascertained that the model is too complex for most questions regarding foot function. It was also pointed out that the method to estimate the load at different sites of the plantar part of the foot had many drawbacks and associated errors, since it consisted of decomposing the estimates of loads from walking trials where only a certain part of the foot landed on a force platform [29].

Abuzzahab [30] presented a three-segment kinetic model of the foot and ankle consisting of the tibia, hindfoot, midfoot and hallux and the validation of the model required kinematic, plantar pressure and ground reaction force data. The model was only validated for the sagittal plane.

Another kinetic foot model is presented by Bruening [31]. This model was created since the already existing kinetic foot models were considered too complex for clinical use. The model includes a shank (tibia and fibula) and three foot segments: hindfoot (calcaneus and talus), forefoot (navicular, cuboid, cuneiforms and metatarsals) and hallux (proximal and distal phalanges). Kinetic parameters were incorporated in the model (by applying ground reaction forces to separate segments, defining the inertial properties and rigidity of the segment), and the joint moments and powers were calculated. The results showed that the model may be used to understand and monitor certain pathologies with only minimal impairments.

2.3.2 Musculoskeletal Foot Models

Musculoskeletal foot models include muscles and/or ligaments, being one of their main purposes to calculate muscle forces in combination with dynamic simulations of motion. As such, musculoskeletal models are used to make predictive simulations by estimating variables that cannot be directly observed and derived.

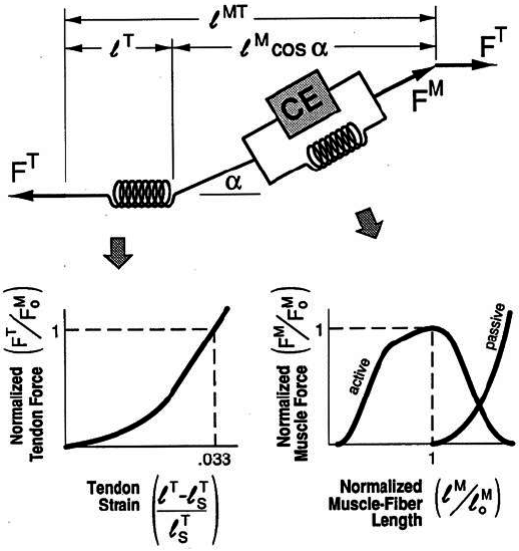

Figure 2.10: Musculotendon actuator model used in the work of Delp [32]. The forces in muscles F^M, and in the tendon F^T, are normalised to peak isometric muscle force F_0^M; while the tendon length l^T and muscle-fiber length l^M are normalised to optimal muscle-fiber length l_0^M. l^{MT} is the musculotendon length, α is the pennation angle and L_s^T is the tendon slack length. Figure adapted from [32]

.

One of the most notable works of the field is that of Delp [32], in which the first musculoskeletal model of the human lower extremity is created to study how the muscle force and moment is affected by surgical interventions. With respect to the foot, an ankle, subtalar and metatarsophalangeal joints were defined. Therefore, the foot model consisted of three rigid segments: the talus, the foot (including the calcaneus, navicular, cuneiforms, cuboid and metatarsals) and the toes (the phalanges). A total of forty-three musculotendon actuators were modelled in the whole body and were represented as line segments with origin, insertion and optional via-points. The muscles were modelled using a three-element Hill model, with a contractile element in parallel with a passive elastic element, both in series with an elastic element. The contractile element modelled the muscle force based on a force-length and force-velocity relation. The parallel element models the elastic behaviour of the muscle, while the series elastic element represents the non-linear tendon behaviour, figure 2.10. Thus, it was possible to compute the force and joint moment that each muscle can develop for the different body positions by combining the musculoskeletal geometric data, the joint models and the musculotendon models [32].

Netptune [33], stresses the importance of examining joint loading during the non-sagittal plane movements and also the individual muscle forces and the ground contact force. In order to do that, the 3D musculoskeletal model of the lower extremity with individual muscle actuators developed by Delp [32] was used and

slightly modified, with the addition of contact elements, in order to split the ground forces per segment. Moreover, the number of muscles included is lower than in the original model of Delp [32], since the muscles were grouped and modelled as fourteen independent muscle groups. Each of them with an origin and insertion point and some of them with additional via points to represent the muscle path more accurately. The force production in muscles was also represented using Hill models. The model was used to analyse ankle sprain injuries.

Anderson and Pandy [34] presented a three dimensional musculoskeletal model of the human body to simulate normal walking. The model was actuated by fifty-four muscles and incorporated twenty-three DOF. Regarding the foot, it was modelled in two segments: hindfoot and toes. The path of the musculotendon actuators is based on the work of Delp [32], and they are also modelled as a 3-element Hill-type muscle in series with a tendon. The results of the model simulation of body segments displacement, ground reaction forces and muscles activations obtained proved to be consistent with literature.

Finally, the most complete and detailed kinematic/kinetic model to date is the Glasgow-Maastricht foot model developed using the Anybody Modelling System [6]. The model has twenty-six segments as it considers each bone a rigid segment, twenty-six joints leading to a forty-six degrees of freedom (DOF) complex. In this study [6], it was possible to recreate the foot motion during the stance phase of a subject. However, specific information on the range of motion of the bony segments is not presented. In the Anybody Wiki page [35], detailed information on the model components is provided, namely the list of ligaments and muscles included in the model. It contains all the major ligament structures and muscles of foot, both intrinsic and extrinsic. Nevertheless, information on the dynamics of the model (joint moments and powers) and muscle forces is not freely available.

2.4 Conclusion

The human foot anatomy is presented, focusing on the foot bones, joints, intrinsic muscles and ligaments, since understanding their anatomy is the first step towards the construction of a musculoskeletal foot model.

An overview of the already existing kinematic, kinetic and musculoskeletal models is provided. The type of foot model developed is fully dependent on its intended use. Kinematic models divide the foot into segments by grouping neighbouring bones together, being their main purpose the study of inter-segment movement through calculation of joint angles. Kinetic models, also known as dynamic models, study the kinetics involved in the generation of movement by calculating, for instance, joint moments and powers. Musculoskeletal models are an extension of dynamic models, as muscles and/or ligaments are incorporated in order to study muscle force and make predictive simulations.

A variety of kinematic and kinetic models, differing on the number of segments is presented. It is observed that most models are divided into segments according to the principal joints of the foot. However, the importance of incorporating a midfoot

segment is broadly conveyed. Regarding musculoskeletal models, the anatomical foot structures included and its level of detail is limited.

It is possible to conclude that biomechanical foot models have been progressively appearing due to the need to better understand the kinematics and forces that cause movement. However, reproducing the real complexity of the foot into a foot model has not been possible yet. Therefore, the development of a more detailed representation contributes to this purpose.

Chapter 3

Methods

Chapter 3 focusses on the methods used to extend and validate the musculoskeletal foot model. After presenting the general work-flow, the different steps of the model construction are explained in detail. Next, the experimental data used for validation and the scaling of the model are explained. Finally, the methods used to validate the model are presented and a brief conclusion is formulated.

Figure 3.1 presents the general work-flow used for the creation and validation of the extended foot model. The first two blocks extend the OpenSim foot model starting from the generic OpenSim gait model by increasing the number of foot segments and DOF, and incorporate the intrinsic muscles and ligaments. The remaining blocks represent the tests preformed to validate the model in terms of its kinematics and dynamics.

The musculoskeletal foot model is developed in OpenSim [36], an open source software used for developing musculoskeletal models and for performing dynamic simulations of movement. Due to the availability of the source code, every user has the possibility to extend the functionality of the software. Furthermore, it provides a platform on which the biomechanical community can build libraries of simulations and models that can be exchanged, analysed and improved [36]. Therefore, OpenSim is the chosen software to develop the extended foot model. The software built-in functionalities can be easily accessed via a graphical user interface, via instruction commands using command prompts or via the MATLAB interface, allowing batch-processing of the analyses.

The generic OpenSim model used as the basis of this work is the *3DGaitModel2392* model [37]. In this model, the foot is modelled in three segments: talus, foot and

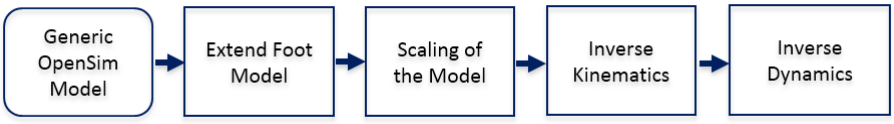

Figure 3.1: Project workflow.

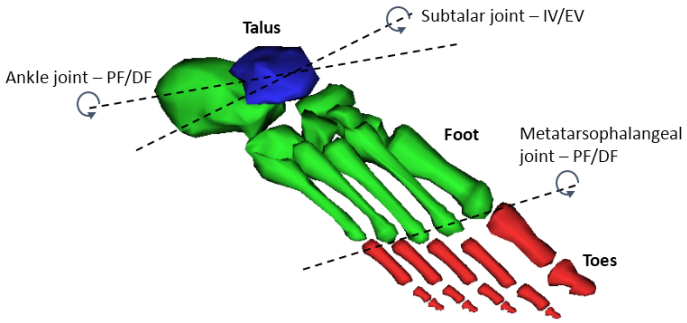

Figure 3.2: The joints and DOF of the 3-segment OpenSim gait model (3DGait-Model2392). Ankle and metatarsophalangeal: plantarflexion/dorsiflexion (PF/DF); subtalar: inversion/eversion (IV/EV).

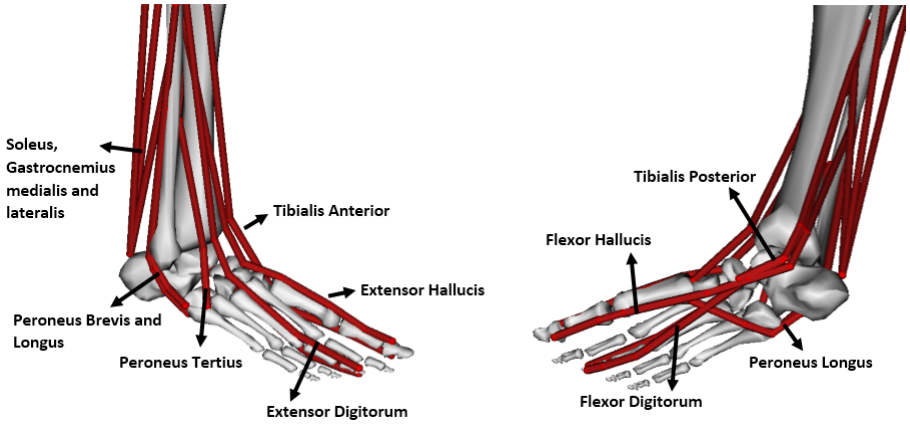

Figure 3.3: Foot extrinsic muscles of the OpenSim gait model (3DGaitModel2392), right foot.

toes. The first segment comprehends only the talus. The second segment, the foot segment, groups the following bones into one rigid body: calcaneus, navicular, cuneiforms, cuboid and metatarsals. Thirdly, the toes segment includes the proximal and distal phalanges. The model incorporates three DOF: plantarflexion/dorsiflexion in the ankle and metatarsophalangeal joints and a combination of eversion-abduction-extension/inversion-adduction-flexion in the subtalar joint, figure 3.2. The model already includes the extrinsic foot muscles, figure 3.3. The muscles of the superficial posterior compartment are the gastrocnemius medialis and lateralis, and the soleus. The deep posterior group comprises the flexor digitorum longus, the flexor hallucis longus and the tibialis posterior. The anterior group includes the tibialis anterior, extensor hallucis longus and extensor digitorum longus. Finally, the lateral compartment is composed of the peroneus brevis, longus and tertius.

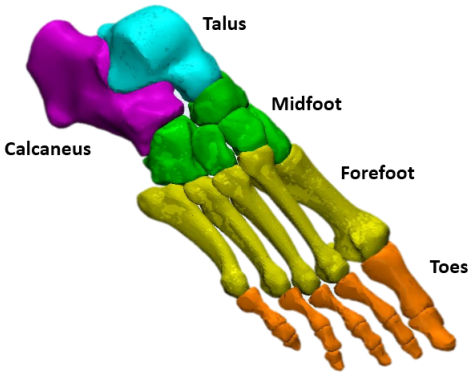

Figure 3.4: The five segments of the extended foot model: calcaneus (purple), talus (blue), midfoot (green), forefoot (yellow) and hallux (orange).

3.1 Model Construction

In order to increase the level of detail of the foot model, the first step comprehends the segments' anatomical division. In parallel, it is necessary to incorporate the architecture of the anatomical structures that span the selected segments: the foot intrinsic muscles and ligaments. Furthermore, it is necessary to acquire the muscles' and ligaments' intrinsic properties.

3.1.1 Number of segments

In the context of the Aladyn project, the KU Leuven Foot and Ankle group (Mechanical Engineering Department, Biomechanics Section) developed a five-segment OpenSim foot model with five joints interconnecting the segments. The definition of these five segments is primarily supported by the location of the principal joints of the foot. Furthermore, it is consistent with the literature's reported need to include a midfoot segment definition [10], [24], [7], [20], to represent the significant movement occurring between the first metatarsal and the navicular [23].

The workflow to create the model comprises the following steps: (1) segmentation of CT scans, using *Matlab*® software (Materialise NV, Belgium); (2) creation of a volume mesh and (3) selection of foot landmarks in *Matlab*® (Materialise NV, Belgium), followed by (4) the attribution of material properties, such as the bone and soft tissue density, in *Matlab*®; thereafter, (5) the anthropometric structure is created in *Matlab*® by computing the total mass, total volume, inertia tensor and centre of mass of each segment; and finally (6) the model is integrated in OpenSim.

Figure 3.4 presents the five segments of the extended foot model: calcaneus, talus, midfoot, forefoot and toes. The midfoot segment includes the cuboid, navicular, and the three cuneiforms (medial, intermedium and lateral). The forefoot segment comprises the five metatarsal bones. Finally, the toes segment consists of all the proximal and distal phalanges. Hence, the five joints interconnecting the segments are the

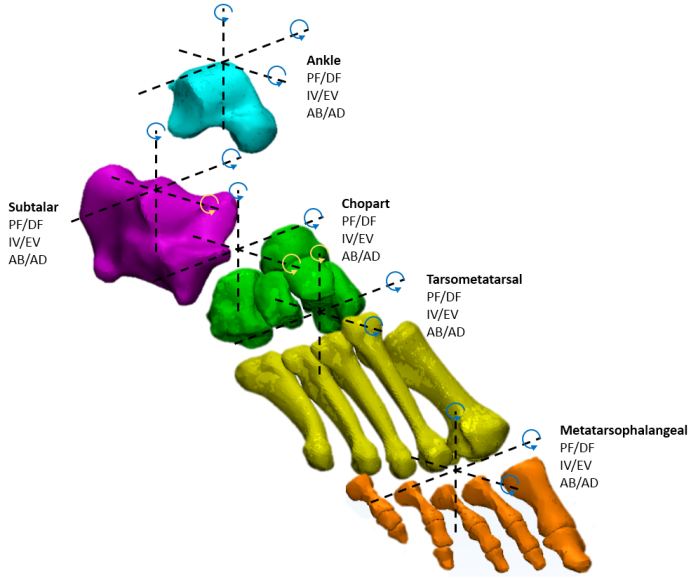

Figure 3.5: The 15 degrees-of-freedom of the 5-segment model. The three rotational movements are incorporated at each joint: plantarflexion/dorsiflexion (PF/DF), inversion/eversion (IV/EV) and abduction/adduction (AB/AD).

ankle (interconnecting the tibia-talus segment), subtalar (talus-calcaneus), chopart (calcaneus-midfoot), tarsometatarsal (midfoot-forefoot) and metatarsophalangeal joint (forefoot-toes).

3.1.2 Number of DOF

The number of degrees-of-freedom that are incorporated in the models depend on the purpose the models are meant to serve. In this particular case, the goal is to provide more insight both in the design of customized insoles and in gait analysis simulations. Therefore, two models were developed based on the five segment model, each consisting of a different number of DOF interconnecting these segments: one model with 15 DOF and another one with 8 DOF was defined.

15 DOF Foot Model

A fifteen DOF model was created with three DOF at each of the five joints, therefore allowing inversion/eversion, plantarflexion/dorsiflexion and abduction/adduction between both the parent (proximal) and child (distal) segment of the joint, figure 3.5. Even though not all these DOF are present in the foot, it was chosen to incorporate a higher level of detail into the model, to evaluate the movements that really occur in the different joints. This way, when performing simulations of movement the behaviour of the foot could give more insight in the joint movement since the rotational movement is not constrained. None of the three translational DOF were incorporated at the joints level.

8 DOF Foot Model

For the 8 DOF model, the attribution of the DOF is based on the anatomical function of the ankle-foot complex, as documented in the work of Hicks [11], figure 2.3. In this sense, the DOF incorporated at the joints are the following:

- Ankle joint: tibia-talus (1 DOF) - plantarflexion/dorsiflexion;
- Subtalar joint: talus-calcaneus (1 DOF) - is defined as an oblique axis, therefore combining eversion-abduction-extension/inversion-adduction-flexion;
- Chopart joint: calcaneus-midfoot (2 DOF) - is defined by two axis, an oblique and an anterior-posterior axis. The first axis, allows a combination of movements between three different planes: eversion-abduction-extension/inversion-adduction-flexion. About the anterior-posterior axis there is eversion with coupled abduction-extension or inversion with coupled adduction-flexion;
- Tarsometatarsal joint: midfoot-forefoot (2 DOF) - is defined by two axis, the 1st ray axis and the 5th ray axis, both allowing flexion-eversion/extension-eversion;
- Metatarsophalangeal joint: forefoot-toes (2 DOF) - plantarflexion/dorsiflexion and abduction/adduction.

3.1.3 Incorporation of Intrinsic Muscles

Understanding and determining the contribution of muscles to the observed motions is an arduous task since muscles can accelerate body segments which they do not span. Therefore, at the foot level, it is important to also include the intrinsic muscles that span the intra-foot joints and that also have an effect on the ankle control.

The incorporation of intrinsic muscles in the OpenSim model started by seeking a more insightful understanding of muscle architecture. It is defined by Kura [18] as *the arrangement of muscle fibers relative to the axis of force generation* and its understanding has significance for, among others, biomechanical modelling and analysis of normal foot function. The physiologic cross-sectional area (PCSA) of the muscle, which measures the number of sarcomeres in parallel with the pull angle of the muscle [1], is considered to be one of the most important parameters since it is believed to be directly related to isometric muscle force [38], [18], which is the force generated by the muscle in a static position without changing its length [39].

The choice of the muscles included in the model was primarily based on the number of segments the muscles span. Hence, only the intrinsic muscles that have their origin, insertion and via points in two or more of the five segments defined in the model were included. Intrinsic muscles within a rigid segment would have no added value, since there is no relative movement and thus no moment generating capacity of the muscle. The geometry and placement of the muscles in the model is based on scientific literature [18], [16], [13]. Figure 3.6 shows the OpenSim extended model with the intrinsic muscles that are included. On the left side, the intrinsic muscles of the dorsal part of the foot as well as the first layer of the plantar intrinsic muscles are

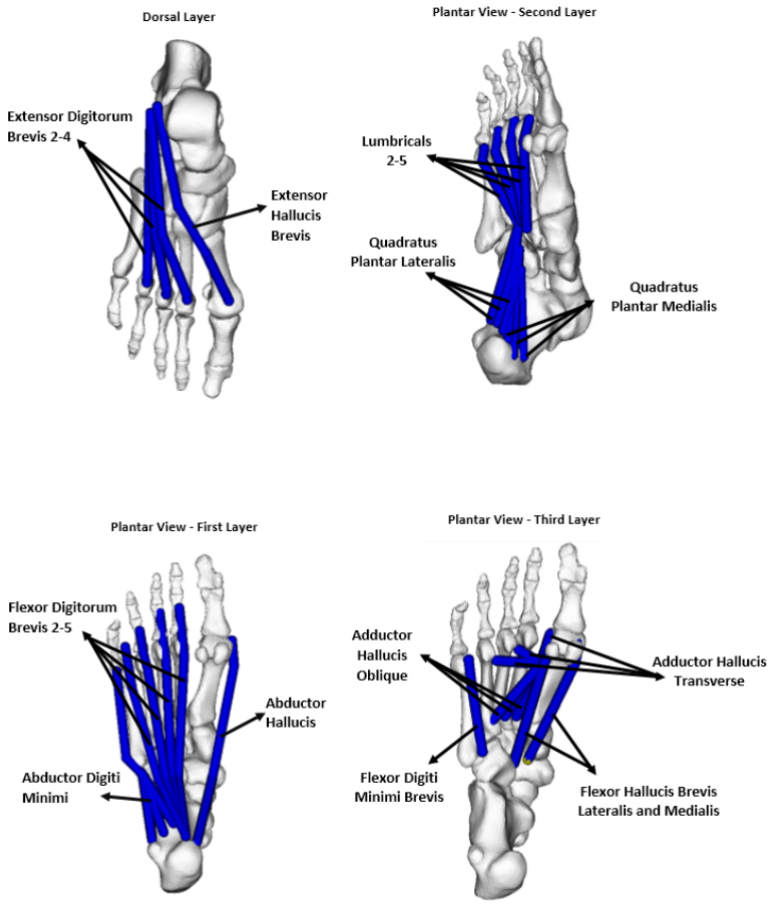

Figure 3.6: Foot intrinsic muscles incorporated in the extended OpenSim model.

presented. The right side shows the second and third layer of the plantar intrinsic muscles. Tables A.2, A.3 and A.4, in Appendix A, list more detailed information on the respective segment where the origin, via and insertion points of the intrinsic muscles are located.

OpenSim provides different classes of muscles, and with each class a different mathematical approach for modelling the muscle functionality. These classes can be very complete, with modelling the force-length and force-velocity behaviour of the muscle structure. However, this requires that specific parameters to describe muscle function, such as the maximum isometric force, the optimal fiber length or the maximum contraction velocity need to be known. However, this information is not freely available in literature. Therefore, it is chosen to model the intrinsic muscles as a simple "Path Actuator". This muscle model describes the muscle force as a ratio of an optimal force transferred to the interconnected bodies via a geometry path. Therefore, this class requires as input the optimal force of the actuator and the geometry path, represented by a set of points (origin, insertion and optional via points). The main reason for using this class is the fact that it allows the creation

of as many path points as needed to define the muscle path, and because it is only required to provide the optimal force of the muscle. These geometrical and muscle force information can be retrieved from literature. It would not be possible to use a different modelling class due to the limited available information on the intrinsic properties of the foot intrinsic muscles, however, for the purposes the extended model is being developed, the path actuator is a fair representation of the intrinsic muscles. In this sense, the parameters used for modelling the path actuators are collected from the work of Kura et al., 1997 since it is one of the very few in depth studies of the intrinsic muscles of the foot. A table with the referred parameters can be found in Appendix A. The integration of all the intrinsic muscles is done in an automated way using $Matlab^{®}$.

3.1.4 Incorporation of Ligaments

Incorporating ligamentous structures in a kinetic foot model significantly increases the level of joint stabilization. Commonly, ligaments are not included in multi-segment foot models, since most models' purpose is to explain muscle function and for that reason ligaments are not included. Nevertheless, ligaments are responsible for stabilizing the foot joints by connecting neighbouring bones together, and will therefore affect the muscle balance.

Ligaments are considered to be viscoelastic structures, meaning that their mechanical behaviour depends on time and on the load-history [40]. The ligaments are passive elements whose primary purpose is to constrain motion. They are gradually stretched as displacement between their origin and insertion points occurs, and return to their original shape when the tension is no longer applied. Ligament behaviour is non-linear as demonstrated by the ligament force-length curves documented when applying constant strain rates [40]. This happens because the collagen fibers that compose the ligaments are recruited gradually as load increases [41]. Figure 3.7 presents the characteristic force-displacement curve of ligaments (also referred to as force-length curve). The force length curve can be subdivided in three regions: the toe region, which is non-linear and occurs for low strain values, the elastic region, which displays a linear behaviour and the plateau region, that leads to failure of the ligament tissue.

The process of incorporating ligaments follows the same work-flow as the incorporation of the intrinsic muscles. The first step consisted of understanding the architecture of the ligaments and their location in the foot. Based on this information, it was possible to decide which ligaments are appropriate to include in the five-segment foot model, since, analogously to the case of the intrinsic muscles, it is only advantageous to include ligaments that span joints that are modelled in the extended OpenSim foot model. The ligament geometry path is described by a point set (origin, insertion and optional via points), in the same way as for the intrinsic muscles.

Figures 3.8 and 3.9 present the ligaments incorporated in the OpenSim foot model. The first figure shows the medial and lateral view of the foot with the respective ligaments. Figure 3.9 presents the ligaments in the plantar aspect of the

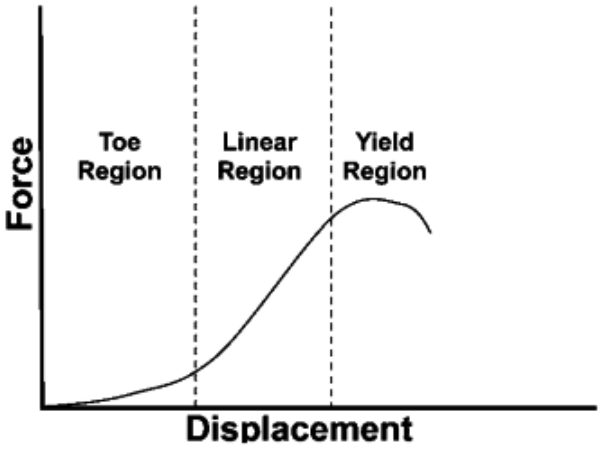

Figure 3.7: Ligament characteristic force-displacement curve. Figure adapted from [42].

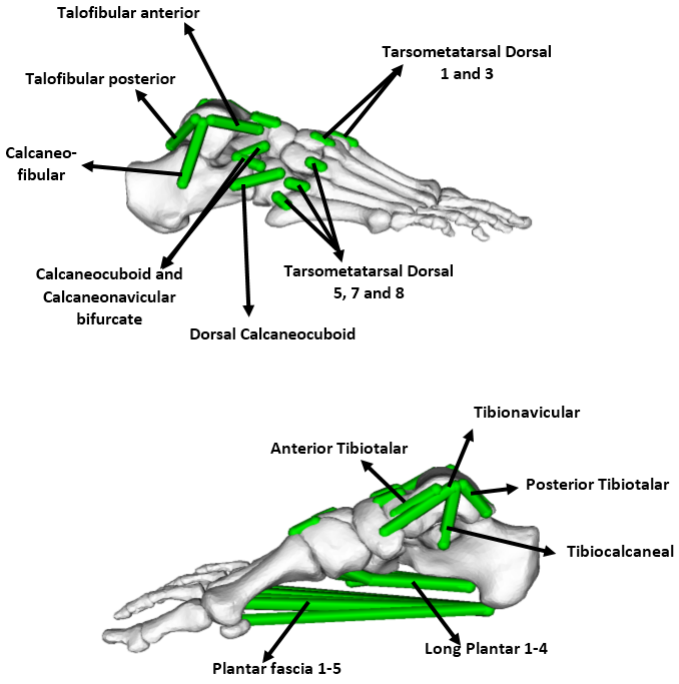

Figure 3.8: Ligaments incorporated in the extended foot model. Lateral and medial views.

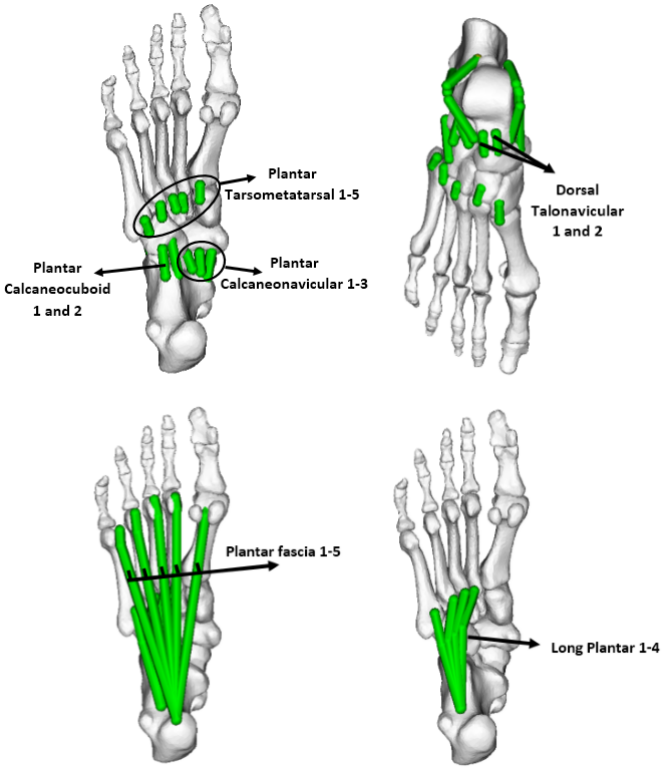

Figure 3.9: Ligaments incorporated in the extended foot model. Plantar and dorsal views.

foot except for the upper right part of the figure that shows the dorsal ligaments that are included in the model. Their placement in the model is according to what is reported in literature [19] [16] [13]. Tables B.2, B.3, B.4 and B.5, in Appendix B, list the ligaments incorporated in the model and the respective body segment to which their origin, via and insertion points are attached to.

In OpenSim it is possible to model ligaments using the class *Ligament*. The class requires as input the resting length of the ligament, which is the length at zero load (zero strain), the force length curve of the ligament and PCSA force, which is used to scale the force-length curve. This force-length curve models the non-linear behaviour of the ligament. It relates the ligament force to the normalized length of the ligament:

$$L_{norm} = \frac{L}{L_0} \tag{3.1}$$

Being L_0 the resting length and L the ligament length.

According to the OpenSim ligament definition, the strain can be written as:

$$\varepsilon = \frac{L - L_0}{L} \tag{3.2}$$

In this way, when the ligament length is shorter than the resting length no force is generated, whereas when the ligament is stretched beyond the resting length, there is force generation.

As mentioned above, the ligament elasticity is generally non-linear. Therefore, it is necessary to construct the ligament force-length curve including the non-linear behaviour. Hence, based on [43], a fourth order polynomial form equation is used to construct the force-length curve:

$$F = A + B\varepsilon + C\varepsilon^2 + D\varepsilon^4 \tag{3.3}$$

Being $A = 0$ and $B = k_{init}$, which is the initial stiffness and the stiffness is defined as: $k = \dfrac{F_1}{\varepsilon * L_0}$. Equation 3.3 is then derived with respect to the strain, 3.4. This way, it is possible to solve the equation for each ligament present in the model, to find the missing variables, C and D.

$$\frac{dF}{d\varepsilon} = B + 2C\varepsilon + 4D\varepsilon^3 \tag{3.4}$$

$$\begin{bmatrix} \varepsilon_{nom}^2 & \varepsilon_{nom}^4 \\ 2\varepsilon_{nom} & 4\varepsilon_{nom}^3 \end{bmatrix} \times \begin{bmatrix} C \\ D \end{bmatrix} = \begin{bmatrix} F_{nom} - k_{init} * \varepsilon_{nom} \\ k_{nom} - k_{init} \end{bmatrix}$$

The parameters that define the non-linearity of the ligament force-length curve are the relative initial stiffness, a_0, and the relative stiffness at nominal strain, a_1. In this sense, the initial stiffness, k_{init}, is scaled by being multiplied by the relative initial stiffness, $a0$ and by the respective resting length, L_0. Similarly, the nominal stiffness, k_{nom}, is multiplied by the relative stiffness at nominal strain, $a1$ and by the ligament resting length, L_0. Therefore, $a0$, defines the slope of the force-length curve at resting length (at the beginning of the curve) interpolating the curve between zero and the linear part of the force length curve, while a_1 interpolates the curve in the yield region [43]. It is then possible to compute the force-length curve of each ligament by interpolating the force values. The force-length curve is normalised by dividing every force value by the PCSA force. It is also important to mention that the yield region of the characteristic ligament force-length curve was modelled to be constant. Table B.1 in Appendix B lists all the values, retrieved from literature [44], [45], [46], [47], [48], [49], [19], that were used as input to the variables mentioned above. The time and load history properties of the ligaments are not taken into account in this approach.

3.2 Experimental Data Collection

Experimental data, collected during the work of Burg [20], was used in order to scale and validate the foot model. The data comprised motion capture data (200 Hz) from five healthy subjects walking barefoot, using ten infra-red Vicon cameras (Vicon ®, Oxford Metrics, UK) to track the motion of a sixty-five skin-mounted marker set. From the sixty-five markers, eighteen are positioned on each foot, figure 3.10, making

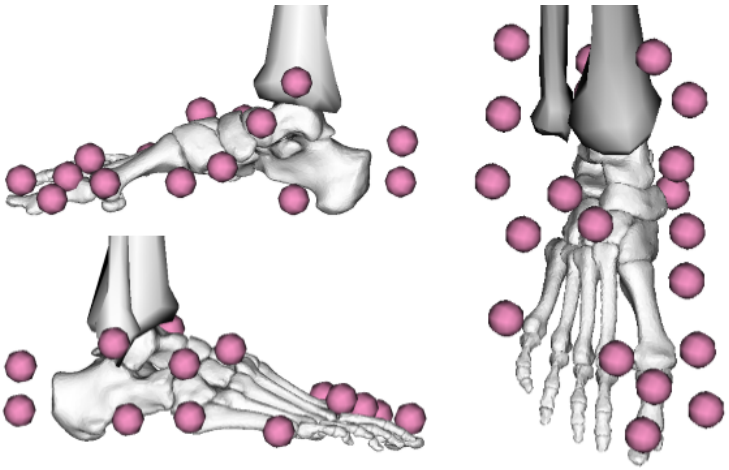

Figure 3.10: Location of the foot markers: right foot.

a total of thirty-six markers focusing on tracking foot motion. Synchronised with the MoCap measurement, plantar pressure data and force data were collected. The force data was collected using two AMTI force plates (Advanced Medical Technology, Watertown, Massachusetts) embedded in the walkway. The plantar pressure plates (RSscan International NV) were positioned on top of these force plates.

3.3 Scaling of the Model

The purpose of scaling the model in OpenSim is to modify the anthropometry and physical dimensions of the generic model in order to match the dimensions of a particular subject. The scaling is performed using the OpenSim scaling tool, which takes the stationary pose of the subject to scale the model. This tool requires as input: the model to be scaled, the mass of the subject, the model marker set and the experimental measured markers during a static pose of the subject. The static pose data file is in *.trc* format (Track Row Column), a format created by Motion Analysis Corporation in order to specify the marker positions in time, during a motion capture trial [50].

It is important to note that there are two different types of markers: the experimental and the model markers. Experimental markers are the skin-mounted markers that are placed on the subject during the motion capture trials. Model markers are placed in the model at the same location as the experimental markers (i.e. at specific anatomical landmarks).

The scaling process consists of determining scale factors by comparing distances between the model markers and the experimental marker positions. Thus, the dimensions of each segment are scaled such that the distances between model marker pairs match the distances between the corresponding experimental marker pairs [51]. Figure 3.11 shows the experimental marker data of one subject in static pose (dark blue) and the model markers (pink). The distance between a pair of model markers

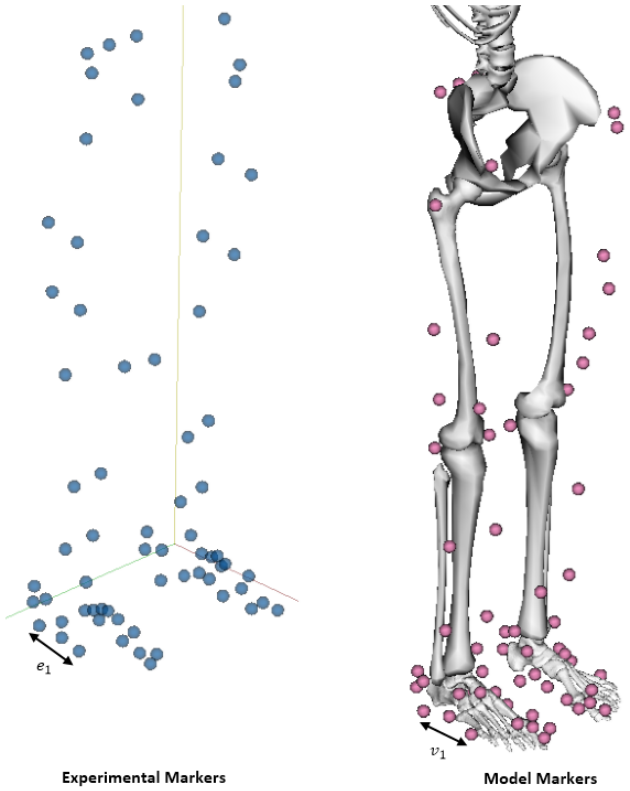

Figure 3.11: Distance between one pair of experimental markers (blue markers, e_1) and one pair of model markers (pink, v_1). The marker distances are used to calculate the scale factor to scale the segments of the model.

(for instance, v_1 in figure 3.11) is calculated by placing the model in the default configuration of OpenSim, while the distance between the experimental markers (e_1 in figure 3.11) is computed by taking the average of the distance of that pair of markers across all frames of the *.trc* file. Hence, the scale factor for this pair of markers equals: $s_1 = e_1/v_1$. The overall scale factor applied to the different segments of the model is then the average of the scale factors of all the pairs. Six marker pairs were defined for each foot, including four pairs between the calcaneus markers and the toes markers, one pair between the base and the head of the metatarsal five, and one pair between the base and the head of the first metatarsal. It was chosen to apply the same scale factor to all the segments in the foot. Furthermore, the masses of the different segments are adjusted so that the total mass equals the subject mass, which is one of the inputs of the OpenSim scaling tool [51].

After scaling, the static pose of the subject is determined. Thereby, the DOF of the model are determined such that the distances between the model markers and the measured markers are minimized. This is performed by a weighted sum of errors, where the weights attributed to the markers determine how strongly the algorithm should try to satisfy this match. Therefore, larger weights penalize errors in order to

match the model markers with the experimental markers more closely [51]. In this sense, larger weights were attributed to the markers located on the shoulders of the subject and on the calcaneus marker cluster.

The path actuators and intrinsic muscles of the model also need to be scaled since these structures depended on the length of the segments. The scaling tool of version 3.2 of OpenSim scales the geometry of these structures, however, it does not scale the length-dependent properties of the ligaments. In a post-processing step, the resting length of the ligaments are scaled in *Matlab*®. Knowing the geometry of the scaled model, the ligament length $L_{ligGeneric}$ and resting length $L_{0Generic}$of the generic model, it is possible to compute the resting length of the scaled model, based on the length of the ligament at default position $L_{ligScaled}$:

$$L_{0Scaled} = \frac{L_{0Generic}}{L_{ligGeneric}} \times L_{ligScaled} \tag{3.5}$$

In the OpenSim scaling tool it is possible to specify if the model markers should be adjusted to match the experimental markers' locations. This is done by loading the same *.trc* file containing the experimental marker locations in order to find the proper set of joint angles to match the subject's pose. It is done by averaging all the experimental markers over the specified time interval and an inverse kinematics problem is solved [52]. Both the 15 DOF and the 8 DOF models were scaled using the same marker set. For the 8 DOF model, the option of adjusting the model markers to the experimental marker location was chosen, while for the 15 DOF model it was not. For the 15 DOF model, the adjusted marker set obtained for the 8 DOF model was used. As a result, the differences observed during inverse kinematics analysis would not be due to differences in scaling. In this way, both models were identically scaled.

3.4 Model Validation

The constructed and scaled model was validated by performing inverse kinematics and inverse dynamics analysis to compare the results with literature. In this sense, the following subsections present the methodologies used to perform the kinematics and dynamics analysis.

3.4.1 Inverse Kinematics

Inverse kinematics analysis estimates joint angles based on measured trajectories of skin-mounted markers. The Kalman Smoother algorithm, by De Groote [53], was the tool used to perform inverse kinematics analysis. Compared to other techniques that estimate joint kinematics, the Kalman Smoother algorithm uses complete marker trajectories to make the estimations instead of basing only on partial marker trajectory information [53]. It computes the joint angles by stepping through each time frame and positioning the model in a pose that best matches the experimental marker and coordinate errors information. It solves a weighted least squares problem and its solution aims at minimizing the marker errors [54].

The Kalman Smoother algorithm consists of two consecutive steps: a Kalman filter to estimate the joint kinematics at a given time instant, t_i, using marker trajectory information only until t_i; and a backward recursion going from the last instant of measured marker trajectory until t_i. Hence, the resulting estimates of the Kalman Smoother are computed based on all the available information. This information includes all the complete marker trajectory, the process model, which describes the expected time evolution of the joint kinematics for each DOF, and the measurement model, which relates the joint kinematics to the measured marker positions [53].

The input needed to run the Kalman Smoother is the experimental marker data collected during the motion capture trials. It is also necessary to provide a scaled musculoskeletal model containing the definition of the marker set used, as well as the weights associated with each marker. The higher the weight of the marker, the more the marker error is minimized. The marker weight attribution is, therefore, a crucial step of the inverse kinematics analysis. It is necessary to assign the foot marker weight differently for each trial, since the reliability of the markers varies from trial to trial, as skin motion artefacts may arise. During the experimental trial there is relative movement of the markers within the segment due to skin motion, thus, the markers that present less displacement throughout the trial are considered more accurate.

The foot marker weights are assigned as follows: for each time step and for each segment, the relative distances between each marker of the segment is calculated. Subsequently, it is possible to calculate the inter-marker distance (IMD) of each pair of markers in one segment by subtracting the minimum distance from the maximum distance observed between those markers. Then, the average IMD for each marker can be calculated. Therefore, for every segment, the average and the maximum values of the IMD were determined. Due to the high number of markers placed on the foot and the consequent difficulties in tracking each marker correctly, the weight range assigned to these markers is limited between 0.25 and 2. The weights are assigned linearly, figure 3.12, being the markers that present the least relative displacement assigned with an higher weight value and the markers presenting more motion with a lower weight. Figure 3.12, is a graphical representation of the weight attribution algorithm. If the maximum IMD of the segment is larger than the upper limit (2 cm) there are two cases: the IMD of the marker is equal or larger than the average IMD, red line, or the IMD of the marker is smaller than the average IMD of the segment, blue line. On the other hand, if the maximum IMD of the segment is equal or smaller than the upper limit there are also two possible cases: the IMD of the marker is equal or larger than the average IMD of the segment, green line, or the IMD of the marker is smaller than the average, blue line. It is important to note that the average IMD varies from segment to segment, therefore it does not have a fixed position in the graph, and it is not necessarily smaller than the upper limit.

Figure 3.13a shows the IMD, in mm, during one trial and figure 3.13b the weight attribution according to the IMD. Regarding the markers of the upper body and leg, the same weight was attributed to all the trials and all the subjects. These markers are assigned a higher weight compared to most of the foot markers, since

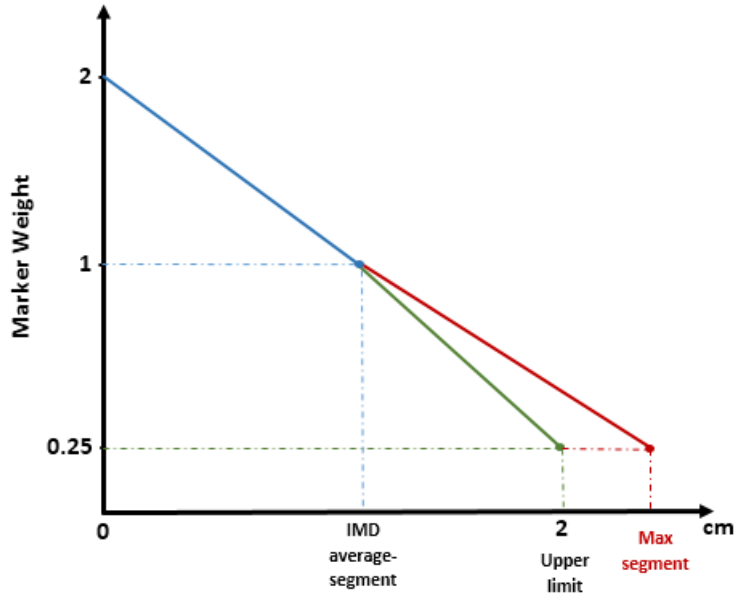

Figure 3.12: Graphical representation of the linear marker weight attribution for the different cases (coloured lines). If the IMD of the segment is larger than an imposed limit (upper limit - 2cm): the blue line represents the weight assignment in case the IMD of the marker is smaller than the average IMD of the segment, and the red line in case the marker IMD is equal or larger than the average IMD of the segment. If, on the other hand, the marker IMD is equal or smaller than the upper limit: the green line in case the marker IMD is equal or larger than the average IMD of the segment and the blue line in the opposite case.

these markers are easily tracked and present small relative displacement during the trials.

Regarding the 15 DOF model, due to having all three rotational degrees-of-freedom in each joint, some of the movements allowed are not anatomically possible. Besides that, the model has more freedom to try to solve the inverse kinematics, generating results that are not, at times, realistic. One of these is the motion of the talus, since skin-mounted markers are not capable of tracking its movement. Therefore, three model markers were added to the model markers' set for the 15 DOF model. The markers were placed on the anterior aspect of the talus; on the lateral aspect and on top of the talus (coinciding with the ankle joint).

After having the resulting motion file obtained from the Kalman Smoother, an extra analysis, named *Body Kinematics*, was performed to retrieve the position and orientation of the bodies with respect to the anatomical planes. It is necessary to perform this extra analysis as the Kalman Smoother retrieves the angles of all the DOF, however, as the 8 and the 15 DOF models have different joint axis definitions, it is not possible to compare the angles. Therefore, by examining the motion relatively to the anatomical planes (sagittal plane- flexion/extension; frontal

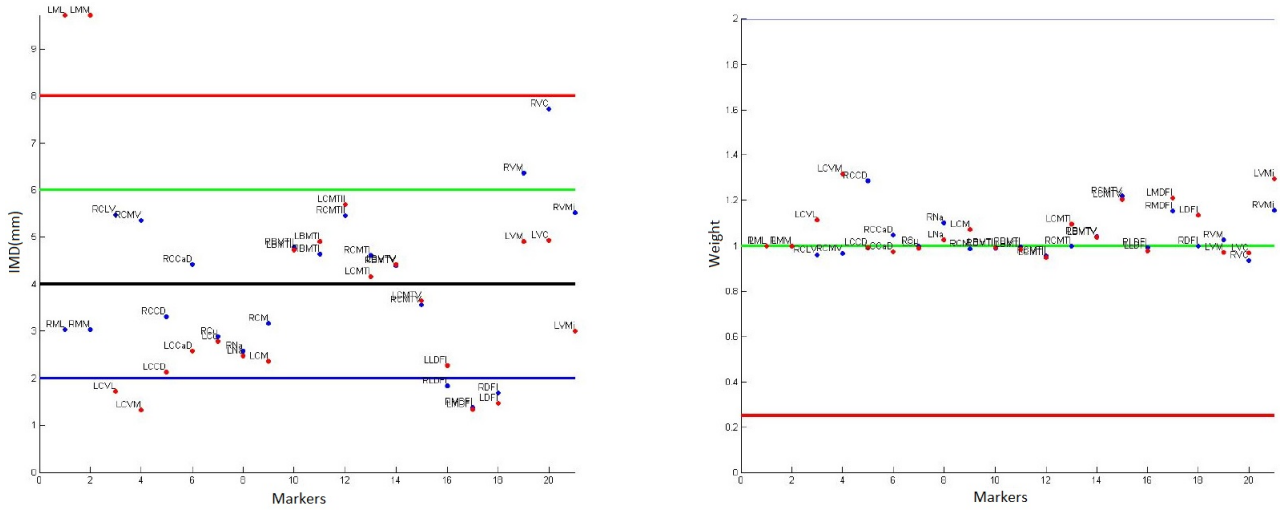

(a) (b)

Figure 3.13: (a) Example of the IMD for one trial and the respective marker weight attribution, (b).

plane- inversion/eversion; transverse plane- adduction/abduction), it is possible to compare both models. Consequently, this analysis calculates the orientation and position of the centre of mass of each body based on the gait pattern calculated via the Kalman Smoother. In this way, by subtracting the orientation of each consecutive pair of segments, it is possible to obtain the relative movement, in degrees, between the segments. This is also the approach used in literature.

The inverse kinematics analysis were performed using the experimental data of five subjects, with four trials per subject. It was done for both the 8 DOF model and the 15 DOF model, and their results were compared. Only the stance phase is studied as it is the most relevant for the purpose of the extended musculoskeletal model, especially to describe the contact of the foot with the ground. For the analysis, right and left foot kinematics were combined for each trial. Therefore, a total of 40 trials is analysed per model: five subjects, four trials per subject and per foot. After observing the output of the inverse kinematics analysis, it was noticed that for some trials the Kalman Smoother algorithm did not find an optimal solution. This was observed for seven out of forty trials (7/40) performed with the 15 DOF model and for four out of forty trials (4/40) with the 8 DOF model. Consequently, it was decided not to take these trials into account. The mean of the different trials per subject was calculated and, subsequently, the mean and standard deviation (SD) of the five subjects were determined.

3.4.2 Inverse dynamics

Inverse dynamics computes the net forces and torques at each joint underlying a particular movement [55]. The inverse dynamics tool of OpenSim was used. It takes the motion (the output of the inverse kinematics) and the external loads applied to the model as input to determine the generalized forces.

The principle behind inverse dynamics is expressed by the classical equation of motion that can be written, in the inverse dynamics sense [56], as follows:

$$M(q)\ddot{q} + C(q, \dot{q}) + G(q) = \tau \tag{3.6}$$

With N the number of degrees-of-freedom, $q, \dot{q}, \ddot{q} \in R^N$ represents the vectors of generalized positions, velocities and accelerations, respectively; $M(q) \in R^{N \times N}$ is the system matrix; $C(q, \dot{q}) \in R^N$ is the vector of Coriolis and centrifugal forces; $G(q) \in R^N$ is the vector of gravitational forces and $\tau \in R^N$ is the vector of generalized forces that must be determined [56]. All the terms of the first part of the equation are known, since the motion of the model is completely defined by the position, orientation, velocity and acceleration of the centre of mass of the segments [56]. Therefore, the inverse dynamics solves the equations of motion in order to find the missing term: the net forces and torques for each joint. In order to maximally exploit the inverse dynamic analyses for the complex foot model, the ground reaction forces need to be split and applied to the respective segments, since the force is acquired as one single vector applied only in one segment.

Splitting the Ground Reaction Forces

It is, therefore, necessary to subdivide the ground reaction forces acting on the foot according to the number of foot segments of the model. The extended foot model consists of five segments, but only four of them are in contact with the ground: more specific, calcaneus, midfoot, forefoot and toes. The subdivision of the ground reaction forces was performed using an algorithm developed by the KU Leuven Foot and Ankle group (Mechanical Engineering Department, Biomechanics Section), based on the plantar pressure data.

The simultaneously measured plantar pressure provides information on the vertical force component and the point of application of this force component. By subdividing the plantar pressure in four regions, figures 3.14a and 3.14b, the vertical force and the point application are subdivided over the four segments. For the two other force components (medio-lateral and antero-posterior), it is assumed that they relate to the measured force with the same ratio as the vertical forces. Therefore, the ground reaction forces are decomposed proportionally to the pressure registered for each segment. The division of the pressure information into the different segments is done manually by selecting four points in the pressure map containing the maximal plantar pressure for all time steps. It is done in a graphical user interface (GUI) in *Matlab*® by choosing four points in the following regions: calcaneus, head of the fifth metatarsal, head of the first metatarsal and toes. Figure 3.14a shows an example of one trial with four chosen points and the consequent division of the segments.

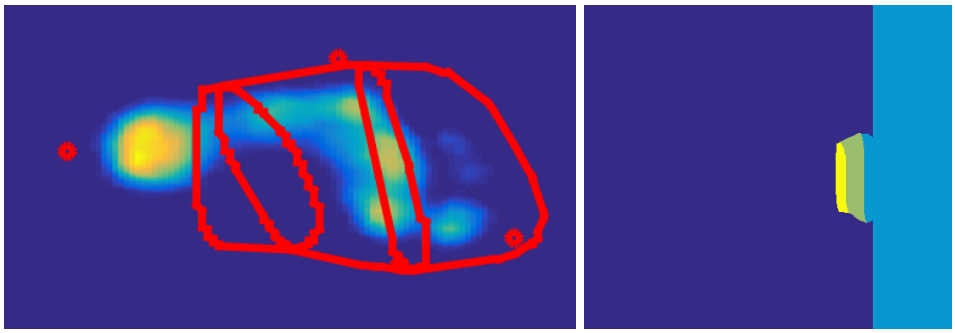

(a) (b)

Figure 3.14: (a) Plantar pressure map for one trial and the segment division based on the selection of four points in the calcaneus, head of the fifth metatarsal, head of the first metatarsal and toes regions. (b) Division of the plantar pressure map regions according to the four foot segments in contact with the floor: calcaneus, midfoot, forefoot and toes.

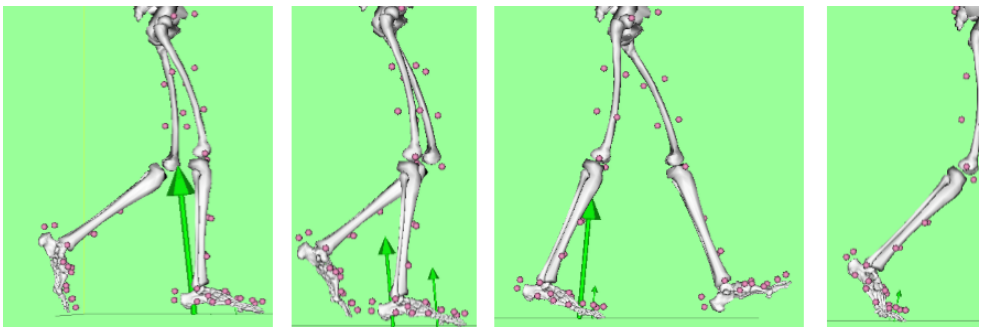

Figure 3.15: Vertical component of the external loads acting on the different foot segments as they contact the ground.

Additionally, figure 3.14b represents the segments' division, being the light blue the region attributed to the toes segment, the green to the forefoot, yellow to the midfoot and the dark blue to the calcaneus.

Therefore, the centre of pressure of each of the four segments is determined based on the pressure data, obtaining a vector acting on the centre of pressure of each segment as it contacts the floor, figure 3.15.

Figure 3.16 shows the decomposition of the vertical forces for the four segments, for one trial.

Joint Moment and Power

During the walking cycle, moments around joints are generated by muscles and ligaments. As defined by Winter [39], *moment of force is the product of a force acting at a distance about an axis of rotation, and which causes an angular acceleration*

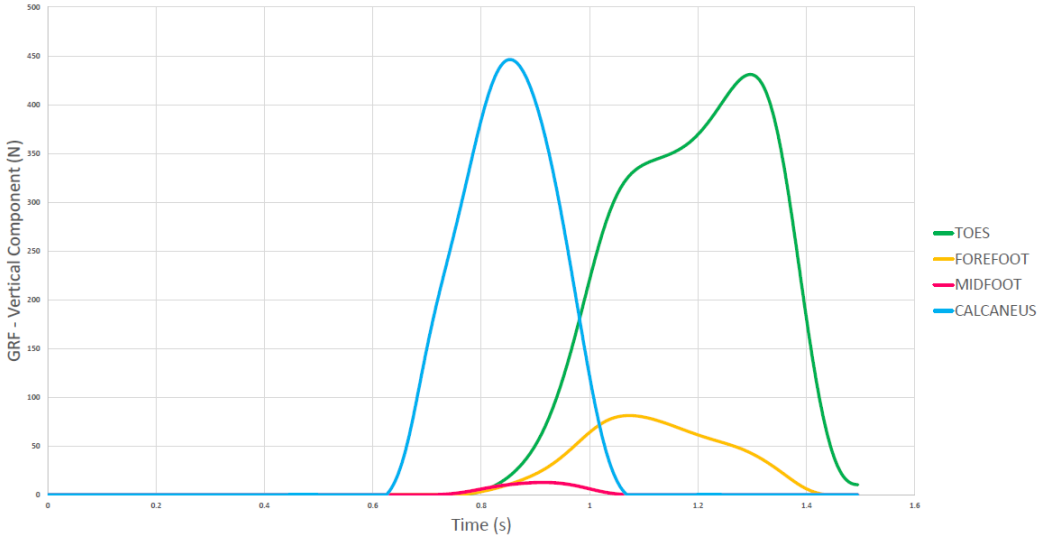

Figure 3.16: Example of the vertical force component of the ground reaction forces acting on the four segments in contact with the ground, for one trial.

about that axis. Hence, the units are Nm and the joint moments of force are defined as *the net result of all internal forces acting at that joint and include the moments due to muscles, ligaments, joint friction and structural constraints* [39]. The joints moments are obtained directly as output of the inverse dynamics analysis.

Power is defined to be energy divided by time and can be expressed as:

$$P = M \times \omega(W) \tag{3.7}$$

With M the moment, and ω the angular velocity. Hence, the units that define Power are $Watt$ or $Joule/s$. In order to calculate the power, it is necessary to know the angular velocity to then multiply it by the moment at each instant. This is obtained by performing a kinematics analysis using the *Analyze* tool of OpenSim, since one of the outputs is the generalized speed. In this sense, it is possible to obtain the joint powers.

Finally, it is important to note that the inverse dynamics analysis was performed for both a model with and without ligaments. This makes it possible to investigate the influence of the ligaments in generating moment and power at the joint level. For each subject, the mean moment and power for the different trials was determined and, subsequently the mean and standard deviation of all five subjects was calculated.

3.5 Conclusion

The methods for extending the generic OpenSim foot model, consisting of three segments and three DOF, included several steps: model construction, scaling and validation. Two five-segment foot models were developed in parallel with this work: an 8 DOF and a 15 DOF model. The five segments are the calcaneus, talus, midfoot

(cuboid, navicular and cuneiformia), forefoot (metatarsals) and toes (phalanges). The foot model was further extended by the incorporation of intrinsic muscles and ligaments. Their location in the foot and characteristic parameters were retrieved from literature and implemented in the OpenSim model in an automated way, using $Matlab^{®}$. The ligament force-length curve was modelled based on literature, taking the form of a fourth order polynomial equation, where the non-linear mechanical behaviour of the ligament was taken into account.

Experimental motion capture, force and plantar data of five healthy subjects, gathered during the work of Burg [20], was used to scale and validate the extended musculoskeletal foot models.

Finally, the methods utilized for the model validation were the inverse kinematics and inverse dynamics analysis. The most optimal marker tracking weight is determined automatically. For the inverse dynamics, the ground reaction forces were subdivided according to the foot segment in contact with the ground, based on plantar pressure data. Given the output of the inverse kinematics (joint angles) and the output of the inverse dynamics (joint moments), the joint powers were calculated.

Chapter 4

Results

The results obtained from the inverse kinematics and inverse dynamics analysis are presented. The first section of the chapter presents the kinematic results both for the 15 DOF model and the 8 DOF model. The next section presents the dynamic results, joint moments and powers, obtained for the 8 DOF model.

4.1 Kinematics

The kinematic results were compared with the results obtained in the study conducted by Lundgren [57]. Their results are considered a golden standard since the kinematic data was collected using in vivo bone-anchored markers. This eliminated the occurrence of skin movement artefacts that is seen using skin-mounted markers. Furthermore, since the marker pins are drilled individually into the foot bones, it is possible to assess the movement between the bones, having a better understanding of the joint motion. Moreover, using this approach, it is possible to track the motion of the talus, which is inaccessible using skin-mounted markers. Nine bones were studied: tibia, fibula, talus, calcaneus, navicular, cuboid, medial cuneiform, first and fifth metatarsal. It is the first in vivo bone-anchored marker study to investigate the movement within the midfoot and forefoot. Nevertheless, as no bone-pins were inserted into the phalanges, the metatarsophalangeal motion was not studied.

Figure 4.1 presents the inverse kinematics results obtained with the 8 DOF model (green), the 15 DOF model (red) and the results of Lundgren [57] (blue). On the X axis the percentage of the stance phase of the gait cycle is displayed and the Y axis represents the angles between the two bodies, in degrees. The first column of figures shows the eversion/inversion rotation, where the positive values correspond to eversion and the negative to inversion. In the second column, the plantarflexion/dorsiflexion movement is shown, being plantarflexion the positive values and dorsiflexion the negative. The third column presents adduction, positive values, and abduction, negative values. The movement, represented by eversion/inversion, plantarflexion/dorsiflexion and abduction/adduction, was calculated for the following pairs of bodies: tibia-talus, talus-calcaneus, calcaneus-midfoot, talus-midfoot, midfoot-forefoot and forefoot-toes. For each subject and each foot, the mean of the

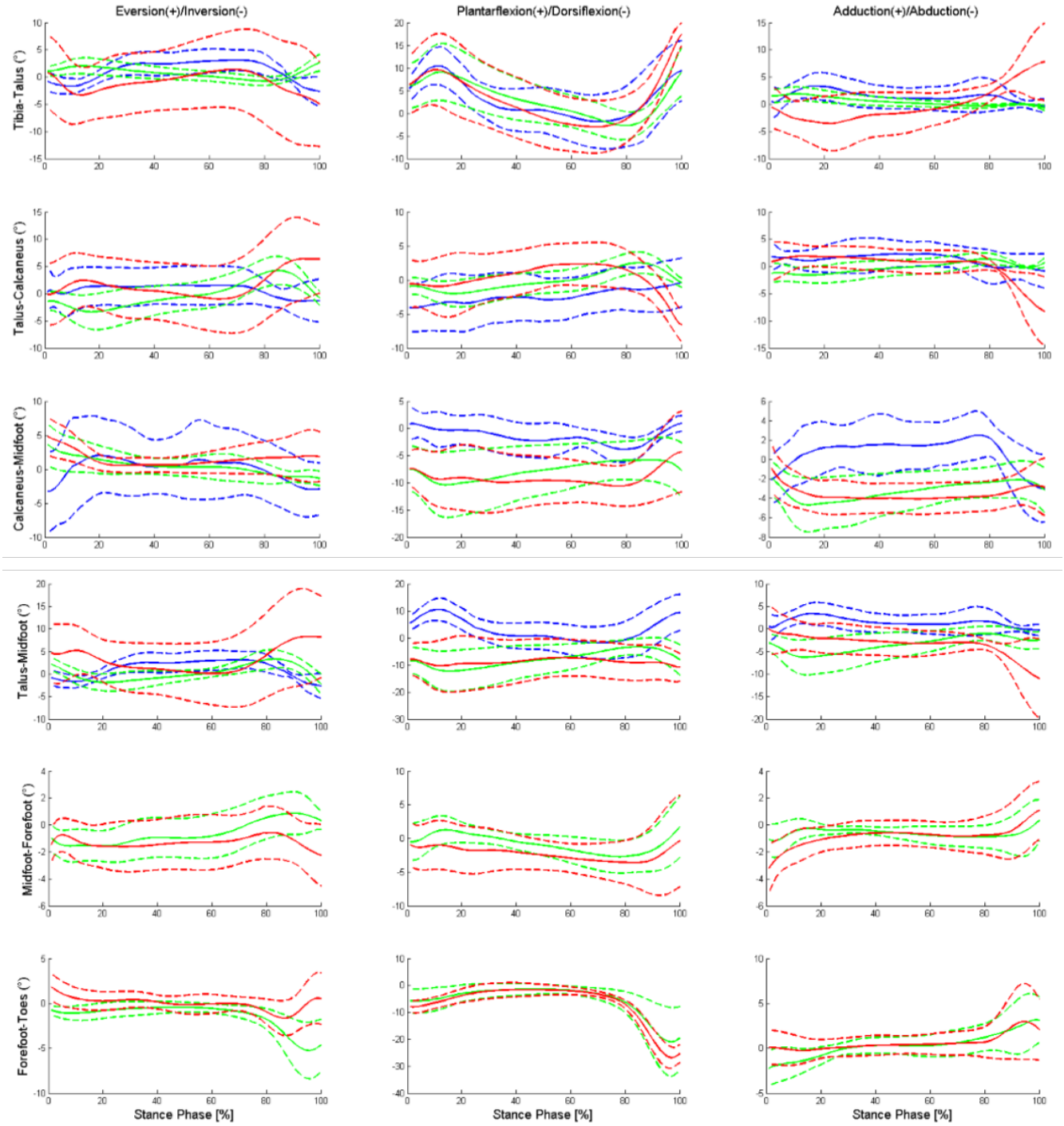

Figure 4.1: Kinematic results obtained with the 8 DOF model (green), with the 15 DOF model (red) and the results from literature [57] (blue). The solid curves represent the mean results of five healthy subjects and the dashed lines ± 1SD.

four trials was calculated. Then, by taking the mean of all trials, the mean and the standard deviation (SD) of all subjects was determined and it is presented in figure 4.1.

Firstly, by inspecting figure 4.1, it is possible to observe that the 15 DOF model (red curves) presents more inter-subject variability and a larger range of motion in most of the plots than the 8 DOF model (green curves), except for the inter-segment joint angles between the forefoot-toes and calcaneus-midfoot segments. Secondly, when comparing the 8 DOF model (green curves) with literature [57] (blue curves), the curve profiles, as well as the range of motion are very consistent. The main differences are observed in the calcaneus-midfoot and talus-midfoot segments. Regarding the calcaneus-midfoot, literature presents a larger range of motion for the eversion/inversion movements, while for the plantarflexion/dorsiflexion and adduction/abduction the curves are somewhat shifted. The same can be found for the talus-midfoot segments. However, it is important to note that the axis scale is rather small, therefore overemphasising the differences between the curves. It is also noteworthy that in literature the comparison is made for the calcaneus in relation to the cuboid, while in the developed models the comparison is between the calcaneus and midfoot. The same happens for the talus and midfoot as in literature the motion is defined between the talus relative to the navicular.

Since the work of Lundgren [57] did not include bone pins in the phalanges, it was not possible to compare the results obtained for the metatarsophalangeal joint. Furthermore, the data of the relative movement of the midfoot-forefoot was not available. Nonetheless, it was possible to compare the results with the work of Burg [20], being the ranges of motion and curve profiles very similar.

4.2 Dynamics

After the kinematic analysis, it was decided to proceed the dynamics analysis with only the 8 DOF model, since this model generated kinematic results that were more comparable to literature. As mentioned in the last chapter, the inverse dynamics analysis was performed for both a model with and without ligaments, allowing to investigate the influence of the ligaments in generating moment and power at the joint level.

Validating the results obtained for the joint moments and powers can only be done with confidence for the ankle joint, since, to date, there are not many other kinetic foot models with such level of detail. Therefore, the ankle joint moment and power were compared with the results obtained by Burg [20].

Figure 4.3 presents the moment normalised by the mass of each subject as a percentage of the gait cycle. The blue curves represent the resulting joint moments taking the ligaments into account and the green curves without considering them.

Observing figure 4.3 and comparing it to the results obtained by Burg [20], figure 4.2, it is possible to state that the profile of the ankle joint curve is in accordance with literature. At the beginning of the stance phase the vertical component of the ground reaction force is aligned with the ankle joint, therefore, a very small moment

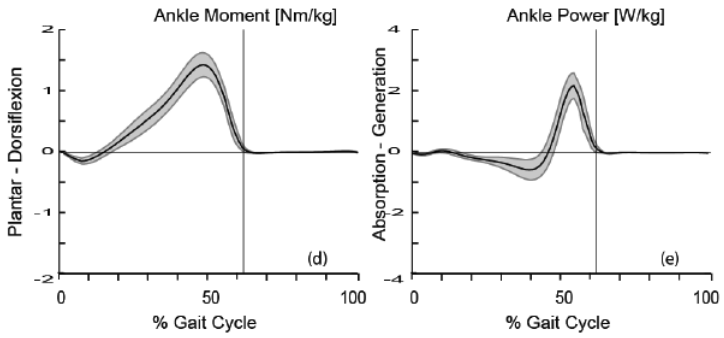

Figure 4.2: Ankle moment and power obtained by Burg [20]. Figure adapted from [20].

(positive in this case) is induced. After that, the moment increases reaching the maximum moment at push off. It is also possible to notice differences in the moment caused by the presence of ligaments, figure 4.3. Only for the ankle and subtalar joint there is no apparent difference.

Figure 4.4 displays the normalised joint power for each one of the eight degrees-of-freedom. Similarly to the moment, the ankle power curve profile follows the patterns found in literature [20]. Negative values indicate power absorption and positive values power generation. The chopart joint, both the oblique and the anterior-posterior axis, stands outs due to presenting an oscillating and somewhat large range of motion. Finally, it is also noteworthy that the axis of the graphs, in figures 4.3 and 4.4, are scaled to different ranges in order to clearly observe the curves' patterns. Nevertheless, the moments and powers are considerably larger at the ankle joint in comparison with the remaining joints.

4.3 Conclusion

Experimental data of five healthy subjects were used to perform the inverse kinematics analysis. The results of the inverse kinematics analysis are very consistent with literature [57] [20]. The most notable dissimilarities were verified between the calcaneus-midfoot and talus-midfoot segments. Regarding the two models in comparison: the 8 DOF model revealed to be more consistent with literature and presented less inter-subject variability.

The 8 DOF model was, therefore, the chosen to continue with the inverse dynamics analysis. The joint moments and powers were compared with literature [20]. The results were also very consistent. When comparing the dynamic results with ligaments and without, it was noticed that for the ankle and the subtalar joint the curve profiles obtained were exactly the same. For the remaining degrees-of-freedom, different moments and powers were verified.

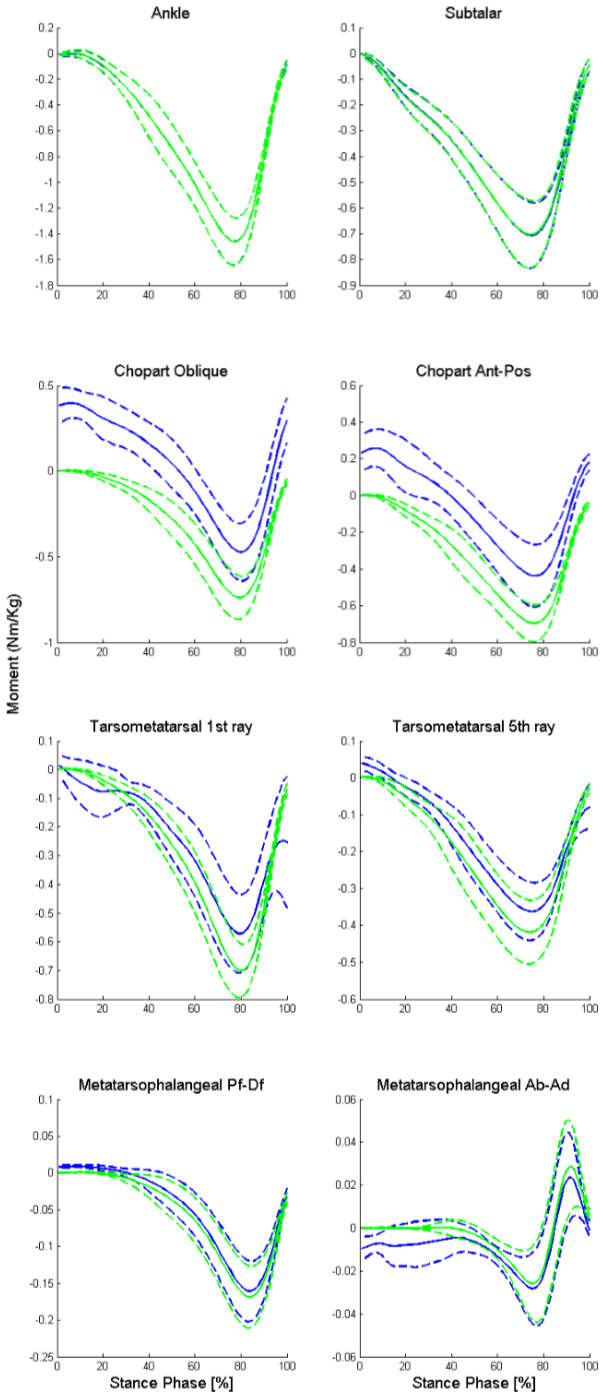

Figure 4.3: Joint normalised moments (Nm/Kg) obtained for the 8 DOF model, with and without including ligaments in the inverse dynamic analysis, blue and green curves, respectively. The solid lines represent the mean moment of the five subjects and the dashed lines ± 1SD.

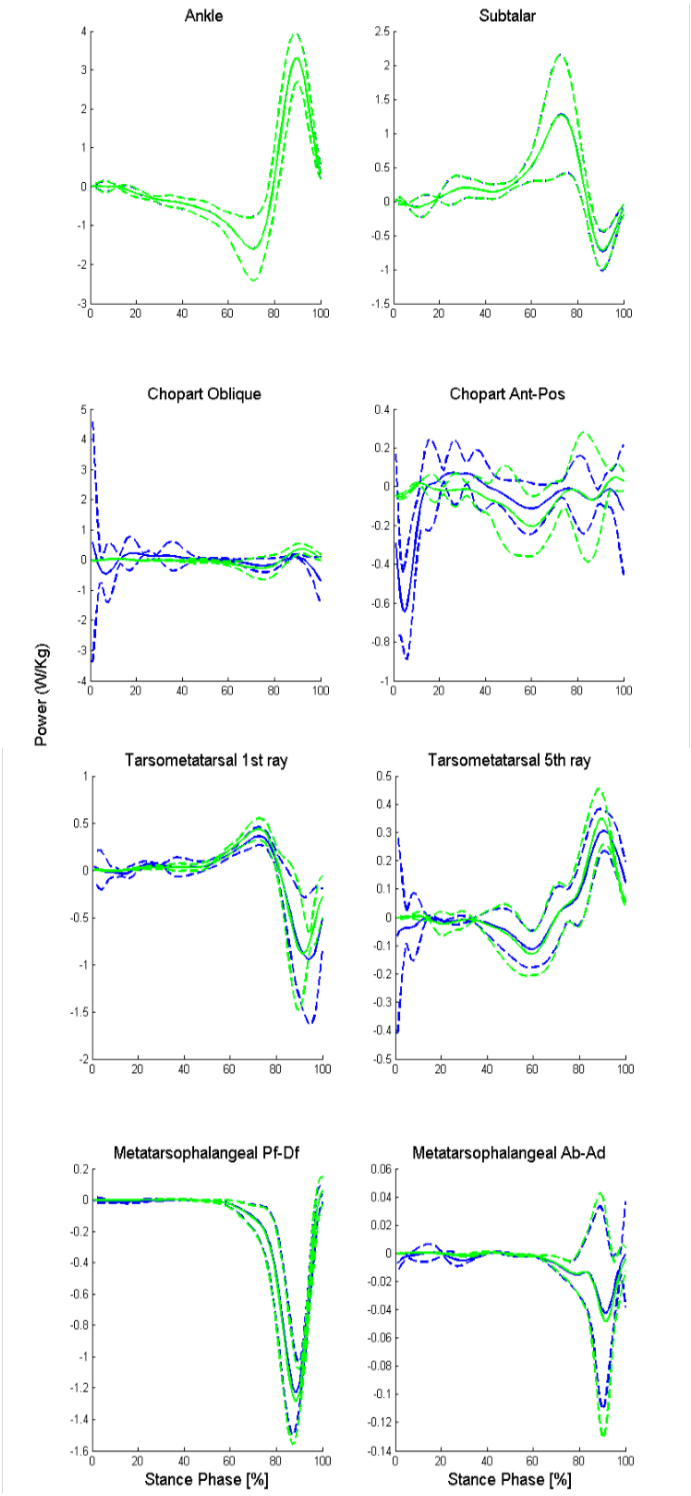

Figure 4.4: Joint powers (W/Kg) obtained for the 8 DOF model, with and without including ligaments in the inverse dynamic analysis, blue and green curves, respectively. The solid lines represent the mean power of the five subjects and the dashed lines ± 1SD.

Chapter 5

Discussion

In this chapter, the results obtained are analysed and discussed. The first section focus on the kinematic results and the required improvements. More specifically, the marker weight attribution and the comparison between the 8 DOF and 15 DOF models are addressed. The next sections discuss the dynamic results. Finally, future developments, such as the static optimization, are briefly presented.

5.1 Kinematics

In this first section, the kinematics behaviour of the extended ankle-foot model is discussed. This comprises first the use of the marker weight attribution for model scaling and inverse kinematics analysis. Secondly, the differences in the inverse kinematics results of the 8 DOF and 15 DOF model are discussed.

Marker Weight Attribution

Experimental testing is commonly subjective to measurement errors, due to equipment limitations as well as human and environment induced errors. During the motion capture data acquisition performed by Burg [20], a high number of experimental markers (18) were placed on the foot in order to track the motion of its bones. This results in two specific challenges: on one hand, a high number of markers need to be placed in an accurate way to track the foot motion; on the other hand, it is challenging to place such a high amount of markers close to each other. This proximity may cause difficulties for the cameras to distinguish the markers. In specific instances, some of the markers are covered either by other markers or by the opposite foot/leg, and are, therefore, not visible to the cameras. Whereas the experimental markers are supposed to be placed in specific anatomical locations, the marker placement is not always accurate and some landmarks are less accessible than others. Furthermore, skin motion artefact also contributes to measurement errors. Ideally, the marker weighting used should accommodate for these effects and differentially attribute marker weights depending on the relative stability of the individual markers. Therefore, an algorithm was developed for determining the tracking weight of individual markers. This was inversely related to the inter-segment

displacement of the marker throughout the trial, as described in chapter 3. It is however important to recognize the high sensitivity of both models to the marker weight attribution during the inverse kinematics analysis. Changes in marker weight were, in some cases, found to have a substantial impact in the result obtained from the Kalman Smoother. Therefore, the weight attribution algorithm can still be improved. As mentioned in the last chapter, for the 15 DOF model, 7 out of 40 trials had to be removed after the kinematics analysis whereas 4 out of 40 trials were removed for the 8 DOF model as the Kalman Smoother could not find a solution for the inverse kinematics. The higher level of measurement error in these trials, introducing noise to the marker data, may be a possible explanation for the failing of these trials. It is also noteworthy that the four trials removed for the 8 DOF model were from the same subject and same foot, hence the problem is more likely to lie in the experimental data acquisition of that particular subject rather than in the model. On the other hand, the removed trials of the 15 DOF model were from different subjects. However, it is also possible that a different weight attribution could have led to better results. Therefore, slightly different weight attribution approaches can be tested in the future. For instance, the maximum displacement distance (upper limit) can be refined. Another option is comparing the IMD of each marker with all the other foot markers instead of comparing them only within the segment.

8 DOF model vs 15 DOF model

Comparing the kinematic results of the 8 DOF model and the 15 DOF model was one of the main objectives of this work. From figure 4.1, it was noticed that the 8 DOF model results are more consistent with literature. The standard deviation obtained is considerably smaller than for the 15 DOF model, meaning that the inter-subject variability is less significant. In this sense, the 8 DOF model produces more consistent results throughout the different subjects.

The calcaneus-midfoot and talus-midfoot movement present the most evident dissimilarity with the data of Lundgren [57]. It is believed that this is due to a different definition of the relative motion: in the work of Lundgren [57] the calcaneus-cuboid motion is compared, whereas in this work the comparison is made between the calcaneus-midfoot. Similarly, Lundgren [57] compares the talus-navicular motion whilst in this work the talus-midfoot motion is compared. Thus, some divergence is expected since the comparison is not made between exactly the same bodies, even though the segments are very close approximations. Added to that, it might also be explained by the fact that no translational displacement is incorporated in either the 8 DOF or 15 DOF models, only the three rotations between segments, and it is possible that minor translational movement occurs between the foot bones during gait. Furthermore, the complexity of accurately tracking the motion of the midfoot using skin-mounted markers can also contribute to the differences verified. When analysing the movement of the chopart joint described by both the 8 DOF and 15 DOF foot models, it was possible to observe a somewhat excessive gap between the midfoot and calcaneus throughout the gait cycle, which is, then, reflected in the kinematic results.

The 15 DOF model presented more variance between trials and subjects, resulting in higher standard deviations when compared with the 8 DOF model and the literature. The 15 DOF model was given freedom to move in all three rotational axis, even if some of those movements are not anatomically correct. By not imposing constraints it was expected that the model would reproduce the real motion occurring at the joints. However, since all the DOF were granted, the resulted movement can be unrealistic by tracking also the measurement noise. Furthermore, currently, it is not possible to track the motion of the talus using skin-mounted markers. While for the 8 DOF model this did not reveal to be a problem, in the 15 DOF model the talus did present considerable unrealistic motion, such as spinning around the calcaneus. To tackle this problem, three markers were added to the model marker set, as mentioned in chapter 3.

Finally, given the arguments mentioned above, the 8 DOF model was the selected to further evaluate the inverse dynamic analysis. Nonetheless, it is important to note that the 15 DOF model is not discarded, instead, it was concluded that further work is needed to improve it. For instance, the incorporation of kinematic constraints, via coordinate coupling or ligament energy, would be a possibility to improve the model. Furthermore, it is also essential to stress that the number of foot segments and DOF incorporated in the model depends on the specific aim of the study.

5.2 Dynamics

The calculated joint moments and powers are consistent with those of the work of Burg [20] for the ankle joint. To date, there are not many dynamic models with sufficient level of detail to provide information on the dynamics of foot joints other than the ankle, making it difficult to compare the results. However, MacWilliams [7] presented joint moment and power results for the ankle, subtalar, calcaneocuboid, tarsometatarsal (medial and lateral) and metatarsophalangeal (hallux, medial and lateral). Even though the joint definition is different from the 8 DOF model, the results are also fairly consistent.

When investigating the role of the ligaments in producing joint moment and power, it was observed that the presence of ligaments does have an impact in moment and power generation. However, for the ankle and subtalar joints the contribution of the ligaments to the moments is minimal. There are several explanations for this result. Firstly, the 8 DOF model only allows one DOF at the ankle and one at the subtalar joint. Thus, looking at figure 5.1a, it can be concluded that the ligaments at the ankle and subtalar joints are almost in the same line of action as those axis, producing a very small moment arm, figure 5.1b. As the magnitude of the moment delivered by the ligament at a joint is determined by the moment arm times the force, the contribution of the ligaments to moment generation is practically null. Additionally, when analysing the ligament forces as an output of the inverse dynamics, the force produced by the ankle and subtalar ligaments is fairly small when compared to the remaining foot ligaments, with a maximum force of 12N.

In order to better understand the effect of the moment arms of the ankle ligaments

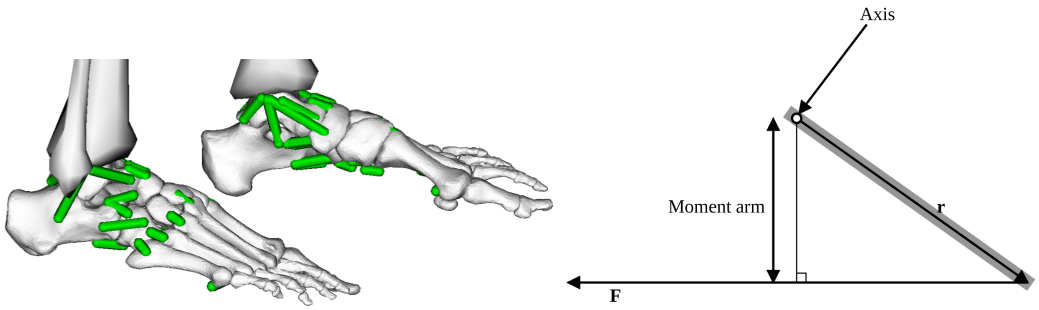

(a) (b)

Figure 5.1: (a) Ligaments of the ankle and subtalar joint incorporated in OpenSim. Their line of action is aligned with the ankle and subtalar axis of the 8 DOF model. (b) Schematic representation of the moment arm, defined as the shortest perpendicular distance from the line of action of a muscle to the joint centre of rotation. Figure adapted from [58].

on the generation of joint moment and power, it was decided to run the inverse dynamics analysis for the 15 DOF model and analyse the moment and power for the other two DOF of the ankle joint. Figure 5.2 presents the moment of the three degrees-of-freedom of the ankle joint for the 15 DOF model and figure 5.3 the power. At the ankle abduction/adduction it is possible to notice a difference between the joint moment and power with and without the ligaments. This corresponds with the clinical findings that the main function of the ankle ligaments is to constrain abduction/adduction. Therefore, their contribution is not observed in the 8 DOF model since this degree-of-freedom is not incorporated. An alternative explanation for the low moment contribution of the ligaments is the fact that the resting length of the ligaments is too large, such that, the ligaments are not stretched beyond the resting length, and, as such, they are not producing force.

Finally, it is also important to mention that when analysing the force-length curve of some ligaments, it was observed that some reach their yielding point, which is not quite realistic since it means the ligament would fail at that point. Consequently, the ligament intrinsic parameters must be revised and refined. Figure 5.4 is an example, showing the force-length curve of the plantar fascia.

Static Optimization

Future research should focus on further elaborating the calculation of individual muscles forces based on the joint moments determined in the inverse dynamics step. A standard technique would be the implementation of static optimization. However, during this work it was noticed that when running a preliminary static optimization, the forces of the reserve actuators were very high. The reserve actuators are torques added to the joints to increase the ability of the model in tracking the measured kinematics. If the sum of the torques produced by the combination of foot muscles

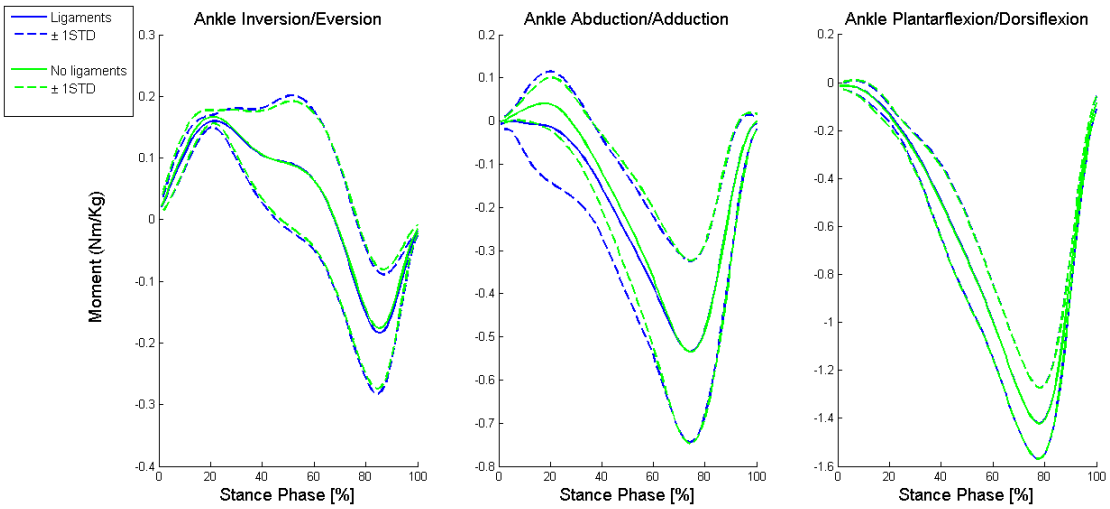

Figure 5.2: Joint moment (Nm/Kg) for the three degrees-of-freedom of the ankle joint of the 15 DOF model, with respect to the percentage of the stance phase. The solid lines represent the mean values of the five subjects and the dashed lines ± 1SD. The blue curves represent the result of the inverse kinematics including the ligaments and the green curves without including them.

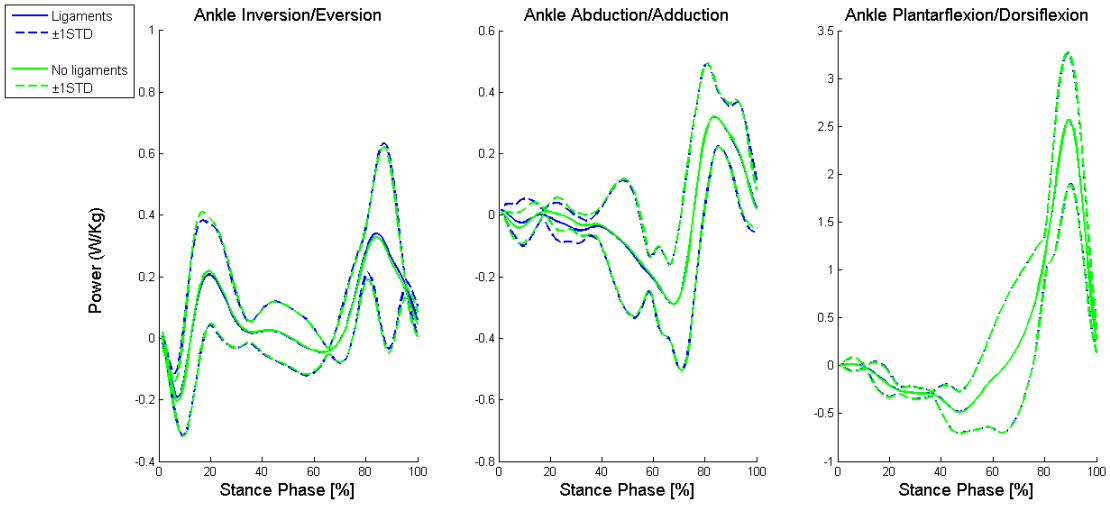

Figure 5.3: Joint power (Nm/Kg) for the three degrees-of-freedom of the ankle joint of the 15 DOF model, with respect to the percentage of the stance phase.

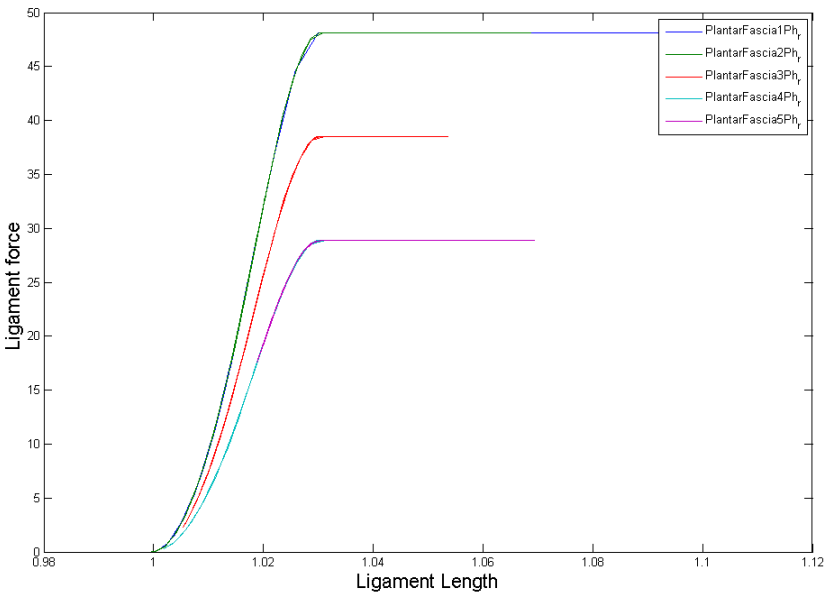

Figure 5.4: Example of the force-length curve of the plantar fascia. The characteristic yield region of the ligament force-length curve was modelled to be constant.

(intrinsic and extrinsic) and ligaments were not able to generate the desired torque, as calculated via the inverse dynamics, the reserve actuators would be active. As such, it is desired that the contribution of the reserve actuation is minimal. Figures 5.5a and 5.5b show that the static optimization cannot find a solution. The solid black line, which represents the result of the inverse dynamics without including the ligaments, should be in between the solid green and red lines, which represent the ligaments' torque plus the minimum and maximum torque of the intrinsic muscles (solid lines) and plus the minimum and maximum torque of both intrinsic and extrinsic muscles (dashed lines). Therefore, since the black lines are not in between the red and green lines, 5.5a and 5.5b, it is possible to conclude that the static optimization cannot find a solution. Consequently, it is necessary to first refine the path actuators and ligaments' parameters before proceeding to the static optimization analysis. The parameter refinement should be done, ideally, based on information collected during experimental measurements of the ligament and intrinsic muscles' characteristics.

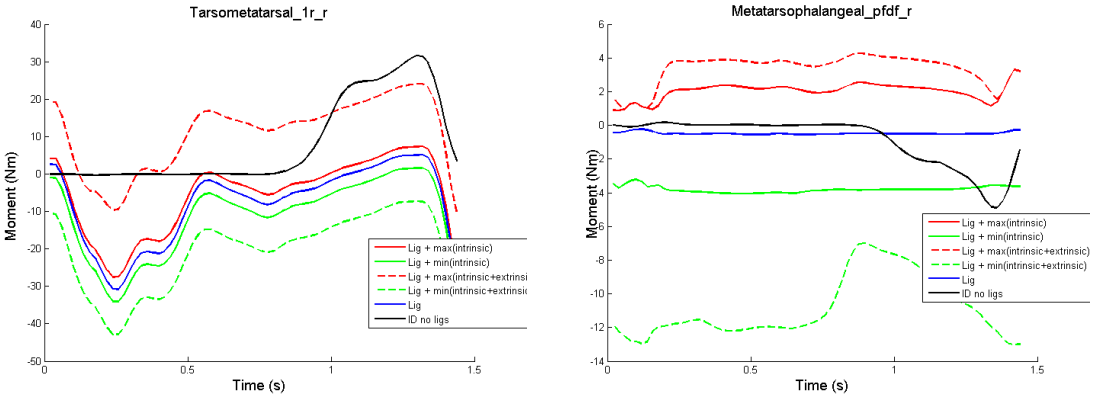

(a) (b)

Figure 5.5: (a) Example of the results of the inverse dynamics for the tarsometatarsal first ray joint and (b) for the metatarsophalangeal plantarflexion/dorsiflexion joint. The solid black line represents the result of the inverse dynamics without ligaments; the solid blue line is the torque produced by the ligaments; the green lines represent the ligaments' torque plus the minimum torque of the intrinsic muscles and plus the minimum torque of both intrinsic and extrinsic muscles; the red lines represent the ligaments' torque plus the maximum torque of the intrinsic muscles and plus the maximum torque of both intrinsic and extrinsic muscles.

Chapter 6

Conclusion

Modelling the true complexity of the ankle-foot is not yet feasible, however, progressively, it is possible to create fair approximations. In this work, an extended ankle-foot musculoskeletal model was developed in OpenSim, responding to the need for a more detailed representation of the ankle-foot complex. This was achieved with the development of two five-segment foot models with 8 and 15 DOF, including thirty intrinsic muscles and thirty-six ligaments. The models' performance in terms of kinematics was compared and validated against literature. Moreover, dynamic analysis were also performed for the 8 DOF model in order to evaluate the joint moments and power and the ligaments' contribution. The current developments allow to provide more extensive insight in the kinematic and kinetic behaviour of the foot in order to aid in the design of customized insoles.

The validation of the foot models proved to be successful as the kinematics and kinetics analysis produced the expected results, according to literature. However, since some experimental trials did not produce optimal results, there are possible improvements to be implemented. Firstly, since errors occur during experimental data acquisition, improving the filtering and treatment of the data is necessary. Secondly, the modelling itself can be improved by, for instance, modelling the translational movement of the joints and not only the rotational movement. Thirdly, the marker weight attribution can also be refined, in order to adapt more accurately to each particular trial. Furthermore, the development of a new marker protocol to better match the needs of the new five-segment foot model is also a possibility.

When analysing the results of the 8 DOF and 15 DOF model, it was possible to conclude that the 8 DOF model is the most fit for the purpose of this project. By following the anatomical functionality of the foot, it was able to generate the most consistent results across the different trials and subjects. On the other hand, the kinematics of the 15 DOF showed excessive variability. It is, however, important to emphasize that with the necessary refinements, the 15 DOF model might reveal to be the most appropriate for a different study, as the DOF incorporated depend on the purpose of the model.

Regarding the incorporation of the intrinsic muscles and ligaments, the characteristic parameters that define them need to be refined. The problematic lies on the lack

of experimental measurements to quantify and characterize these parameters for some of the muscles and ligaments, such as the ligament resting length, nominal stiffness or the intrinsic muscles' contraction velocity. Therefore, the parameters retrieved from literature, for some cases, were mere approximations and not experimentally obtained values. Consequently, as verified when analysing the results, the behaviour of some ligaments (force-length curve) was rather unrealistic. Nonetheless, evaluating the contribution of the ligaments to joint moment and power generation, minor contributions were found at the level of the ankle joint, however a larger effect was found at the midfoot and forefoot joints. The calculation of individual muscle forces, the next step of the work-flow, would rely on tuning the parameters of the intrinsic muscles and ligaments.

Furthermore, future work will also consist on performing forward simulation analysis in order to verify the model performance in reproducing the plantar pressure profiles with the use of a contact model.

Appendices

Appendix A

Intrinsic Muscles

Table A.1 presents the input parameters for modelling the foot intrinsic muscles in OpenSim as *Path Actuators*. Tables A.2, A.3 and A.4 present their respective geometry path.

Table A.1: Parameters of the foot intrinsic muscles.

Muscle Name	Isometric Force	PCSA
Abductor Hallucis	301.76	6.68
Extensor Hallucis Brevis	60.53	1.34
Abductor Digiti Minimi 1, 2 and 3	57.07	1.26
Lumbrical 2 and 3	18.07	0.4
Lumbrical 4	13.55	0.3
Lumbrical 5	8.13	0.18
Quadratus Plantar Medialis	29.51	0.65
Quadratus Plantar Lateralis	15.06	0.33
Flexor Digitorum Brevis 2	80.41	1.78
Flexor Digitorum Brevis 3	67.31	1.49
Flexor Digitorum Brevis 4	56.92	1.26
Flexor Digitorum Brevis 5	15.81	0.35
Extensor Digitorum Brevis 2	35.69	0.79
Extensor Digitorum Brevis 3	23.04	0.51
Extensor Digitorum Brevis 4	19.88	0.44
Adductor Hallucis Oblique	74.39	1.65
Adductor Hallucis Transverse	9.34	0.21
Flexor Digiti Minimi Brevis	90.35	2
Flexor Hallucis Brevis Medialis	81.31	1.8
Flexor Hallucis Brevis Lateralis	95.77	2.12

Table A.2: Geometry path of the intrinsic muscles - part 1.

Muscle Name	Point	Body	Model Segment
Abductor Hallucis	Origin	Calcaneus	Calcaneus
	Via	Navicular	Midfoot
	Via	Metatarsal	Forefoot
	Insertion	ProximalPhalange1	Toes
Extensor Hallucis Brevis	Origin	Calcaneus	Calcaneus
	Via	Intermediate Cuneiform	Midfoot
	Via	Metatarsal1	Forefoot
	Insertion	ProximalPhalange	Toes
Abductor Digiti Minimi1	Origin	Calcaneus	Calcaneus
	Via	Metatarsal5	Forefoot
	Via	Metatarsal5	Forefoot
	Insertion	ProximalPhalange5	Toes
Abductor Digiti Minimi2	Origin	Calcaneus	Calcaneus
	Via	Metatarsal5	Forefoot
	Via	Metatarsal5	Forefoot
	Insertion	ProximalPhalange5	Toes
Abductor Digiti Minimi3	Origin	Calcaneus	Calcaneus
	Via	Metatarsal5	Forefoot
	Via	Metatarsal5	Forefoot
	Insertion	ProximalPhalange5	Toes
Lumbrical2	Origin	FlexorDigitorumLongusTendon	Midfoot
	Via	Metatarsal2	Forefoot
	Insertion	ProximalPhalange2	Toes
Lumbrical3	Origin	FlexorDigitorumLongusTendon	Midfoot
	Via	Metatarsal3	Forefoot
	Insertion	ProximalPhalange3	Toes
Lumbrical4	Origin	FlexorDigitorumLongusTendon	Midfoot
	Via	Metatarsal4	Forefoot
	Insertion	ProximalPhalange4	Toes
Lumbrical5	Origin	FlexorDigitorumLongusTendon	Midfoot
	Via	Metatarsal5	Forefoot
	Insertion	ProximalPhalange5	Toes
Quadratus Plantar Medialis1	Origin	Calcaneus	Calcaneus
	Insertion	FlexorDigitorumLongusTendon	Midfoot

Table A.3: Geometry path of the intrinsic muscles - part 2.

Muscle Name	Point	Body	Model Segment
Quadratus Plantar Medialis2	Origin	Calcaneus	Calcaneus
	Insertion	FlexorDigitorumLongusTendon	Midfoot
Quadratus Plantar Medialis3	Origin	Calcaneus	Calcaneus
	Insertion	FlexorDigitorumLongusTendon	Midfoot
Quadratus Plantar Lateralis1	Origin	Calcaneus	Calcaneus
	Insertion	FlexorDigitorumLongusTendon	Midfoot
Quadratus Plantar Lateralis2	Origin	Calcaneus	Calcaneus
	Insertion	FlexorDigitorumLongusTendon	Midfoot
Quadratus Plantar Lateralis3	Origin	Calcaneus	Calcaneus
	Insertion	FlexorDigitorumLongusTendon	Midfoot
Flexor Digitorum Brevis2	Origin	Calcaneus	Calcaneus
	Via	Cuboid	Midfoot
	Via	Metatarsal2	Forefoot
	Via	ProximalPhalange2	Toes
	Insertion	MiddlePhalange2	Toes
Flexor Digitorum Brevis3	Origin	Calcaneus	Calcaneus
	Via	Cuboid	Midfoot
	Via	Metatarsal3	Forefoot
	Via	ProximalPhalange3	Toes
	Insertion	MiddlePhalange3	Toes
Flexor Digitorum Brevis4	Origin	Calcaneus	Calcaneus
	Via	Cuboid	Midfoot
	Via	Metatarsal4	Forefoot
	Via	ProximalPhalange4	Toes
	Insertion	MiddlePhalange4	Toes
Flexor Digitorum Brevis5	Origin	Calcaneus	Calcaneus
	Via	Cuboid	Midfoot
	Via	Metatarsal5	Forefoot
	Insertion	MiddlePhalange5	Toes
Extensor Digitorum Brevis2	Origin	Calcaneus	Calcaneus
	Via	Metatarsal3	Forefoot
	Via	Metatarsal2	Forefoot
	Via	Metatarsal2	Forefoot

Table A.4: Geometry path of the intrinsic muscles - part 3.

Muscle Name	Point	Body	Model Segment
Extensor Digitorum Brevis3	Origin	Calcaneus	Calcaneus
	Via	Metatarsal3	Forefoot
	Via	Metatarsal3	Forefoot
	Via	Metatarsal3	Forefoot
Extensor Digitorum Brevis4	Origin	Calcaneus	Calcaneus
	Via	Metatarsal4	Forefoot
	Via	Metatarsal4	Forefoot
Adductor Hallucis Oblique1	Origin	Metatarsal2	Forefoot
	Via	Metatarsal1	Forefoot
	Insertion	Proximal Phalange1	Toes
Adductor Hallucis Oblique2	Origin	Metatarsal3	Forefoot
	Via	Metatarsal1	Forefoot
	Insertion	Proximal Phalange1	Toes
Adductor Hallucis Oblique3	Origin	Metatarsal4	Forefoot
	Via	Metatarsal1	Forefoot
	Insertion	Proximal Phalange1	Toes
Adductor Hallucis Transverse1	Origin	Metatarsal3	Forefoot
	Via	Metatarsal1	Forefoot
	Insertion	Proximal Phalange1	Toes
Adductor Hallucis Transverse2	Origin	Metatarsal4	Forefoot
	Via	Metatarsal1	Forefoot
	Insertion	Proximal Phalange1	Toes
Flexor Digiti Minimi Brevis	Origin	Metatarsal5	Forefoot
	Via	Metatarsal5	Forefoot
	Insertion	Proximal Phalange5	Toes
Flexor Hallucis Brevis Medialis	Origin	Navicular	Midfoot
	Via	Metatarsal1	Forefoot
	Via	Metatarsal1	Forefoot
	Insertion	Proximal Phalange1	Toes
Flexor Hallucis Brevis Lateralis	Origin	Navicular	Midfoot
	Via	Metatarsal1	Forefoot
	Via	Metatarsal1	Forefoot
	Insertion	Proximal Phalange1	Toes

Appendix B

Ligaments

Table B.1 presents the input parameters for modelling the foot ligaments in OpenSim. Tables B.2, B.3, B.4 and B.5 present their respective geometry path.

Table B.1: Parameters of the foot ligaments.

Ligament Name	Resting Length L_0 (m)	Nominal Strain ε	Nominal Force F (N)	Relative Initial Stifness k_{init}	Relative stiffness at nominal strain k_{nom}	Nominal Stifness k (N/m)
TibioTalarPost	0.023	0.125	39.14	0.25	3.8	13855.14
TibioTalarAnt	0.029	0.125	19.56	0.26	2.85	5415.48
TibioCalcaneal	0.034	0.083	18.97	0.2	4.1	6648.50
TibioNavicular	0.047	0.125	450.00	1	1	77374.76
TaloFibularPost	0.034	0.083	4.53	0.14	4.15	1590.75
TaloFibularAnt	0.034	0.175	47.53	0.3	2.51	7895.51
CalcaneoFibular	0.041	0.083	10.12	0.1	3.8	2995.20
PlantarFascia1Ph	0.163	0.036	62.74	0.6	1.5	10694.89
PlantarFascia2Ph	0.164	0.036	62.74	0.6	1.5	10609.67
PlantarFascia3Ph	0.163	0.036	50.19	0.6	1.5	8528.85
PlantarFascia4Ph	0.155	0.036	37.64	0.6	1.5	6736.18
PlantarFascia5Ph	0.146	0.036	37.64	0.6	1.5	7155.45
LongPlantar1	0.092	1.000	5383.13	1	1	58730.56
LongPlantar2	0.087	1.000	4037.34	1	1	46185.92
LongPlantar3	0.082	1.000	2691.56	1	1	32996.03
LongPlantar4	0.073	1.000	1345.78	1	1	18472.40
CalcaneoNavicularPlantar1	0.022	1.000	1032.85	1	1	46019.95
CalcaneoNavicularPlantar2	0.014	1.000	1200.00	1	1	86692.61
CalcaneoNavicularPlantar3	0.012	1.000	1200.00	1	1	101095.88
CalcaneoCuboidPlantar1	0.020	1.000	1500.00	1	1	74419.53
CalcaneoCuboidPlantar2	0.026	1.000	1500.00	1	1	57284.57
CalcaneoCuboidDorsal	0.029	1.000	1032.85	1	1	35615.38
TaloNavicularDorsal1	0.013	1.000	500.00	1	1	37683.63
TaloNavicularDorsal2	0.013	1.000	500.00	1	1	37683.60
CalcaneoNavicularBifurcate	0.019	1.000	1032.85	1	1	54608.87
CalcaneoCuboidBifurcate	0.016	1.000	1032.85	1	1	63712.04
TarsoMetatarsalDorsal1	0.014	1.000	500.00	1	1	34498.41
TarsoMetatarsalDorsal3	0.011	1.000	500.00	1	1	45524.49
TarsoMetatarsalDorsal5	0.008	1.000	200.00	1	1	25625.19
TarsoMetatarsalDorsal7	0.010	1.000	500.00	1	1	51428.32
TarsoMetatarsalDorsal8	0.008	1.000	500.00	1	1	59842.86
TarsoMetatarsalPlantar1	0.010	1.000	1032.00	1	1	100199.82
TarsoMetatarsalPlantar2	0.008	1.000	20913.46	1	1	2462555.57
TarsoMetatarsalPlantar3	0.008	1.000	20913.46	1	1	2629730.45
TarsoMetatarsalPlantar4	0.009	1.000	500.00	1	1	57175.35
TarsoMetatarsalPlantar5	0.010	1.000	500.00	1	1	48895.98

Table B.2: Ligaments' geometry path - part 1.

Ligament	Point	Body	Model Segment
TibioTalarPost	Origin	Tibia	Tibia
	Insertion	Talus	Talus
TibioTalarAnt	Origin	Tibia	Tibia
	Insertion	Talus	Talus
TibioCalcaneal	Origin	Tibia	Tibia
	Insertion	Calcaneus	Calcaneus
TibioNavicular	Origin	Tibia	Tibia
	Insertion	Navicular	Midfoot
TaloFibularPost	Origin	Tibia	Tibia
	Insertion	Talus	Talus
TaloFibularAnt	Origin	Tibia	Tibia
	Insertion	Talus	Talus
CalcaneoFibular	Origin	Tibia	Tibia
	Insertion	Calcaneus	Calcaneus
PlantarFascia1Ph	Origin	Calcaneus	Calcaneus
	Via	Metatarsal1	Forefoot
	Insertion	ProximalPhalange1	Toes
PlantarFascia2Ph	Origin	Calcaneus	Calcaneus
	Via	Metatarsal2	Forefoot
	Insertion	ProximalPhalange2	Toes
PlantarFascia3Ph	Origin	Calcaneus	Calcaneus
	Via	Metatarsal3	Forefoot
	Insertion	ProximalPhalange3	Toes

Table B.3: Ligaments' geometry path - part 2.

Ligament	Point	Body	Model Segment
PlantarFascia4Ph	Origin	Calcaneus	Calcaneus
	Via	Metatarsal4	Forefoot
	Insertion	ProximalPhalange4	Toes
PlantarFascia5Ph	Origin	Calcaneus	Calcaneus
	Via	Metatarsal5	Forefoot
	Insertion	ProximalPhalange5	Toes
LongPlantar1	Origin	Calcaneus	Calcaneus
	Via	Cuboid	Midfoot
	Insertion	Metatarsal2	Forefoot
LongPlantar2	Origin	Calcaneus	Calcaneus
	Via	Cuboid	Midfoot
	Insertion	Metatarsal3	Forefoot
LongPlantar3	Origin	Calcaneus	Calcaneus
	Via	Cuboid	Midfoot
	Insertion	Metatarsal4	Forefoot
LongPlantar4	Origin	Calcaneus	Calcaneus
	Via	Cuboid	Midfoot
	Insertion	Metatarsal5	Forefoot
CalcaneoNavicularPlantar1	Origin	Calcaneus	Calcaneus
	Insertion	Navicular	Midfoot
CalcaneoNavicularPlantar2	Origin	Calcaneus	Calcaneus
	Insertion	Navicular	Midfoot
CalcaneoNavicularPlantar3	Origin	Calcaneus	Calcaneus
	Insertion	Navicular	Midfoot

Table B.4: Ligaments' geometry path - part 3.

Ligament	Point	Body	Model Segment
CalcaneoCuboidPlantar1	Origin	Calcaneus	Calcaneus
	Insertion	Cuboid	Midfoot
CalcaneoCuboidPlantar2	Origin	Calcaneus	Calcaneus
	Insertion	Cuboid	Midfoot
CalcaneoCuboidDorsal	Origin	Calcaneus	Calcaneus
	Insertion	Cuboid	Midfoot
TaloNavicularDorsal1	Origin	Talus	Talus
	Insertion	Navicular	Midfoot
TaloNavicularDorsal2	Origin	Talus	Talus
	Insertion	Navicular	Midfoot
CalcaneoNavicularBifurcate	Origin	Calcaneus	Calcaneus
	Insertion	Navicular	Midfoot
CalcaneoCuboidBifurcate	Origin	Calcaneus	Calcaneus
	Insertion	Cuboid	Midfoot
TarsoMetatarsalDorsal1	Origin	Medial Cuneiform	Midfoot
	Insertion	Metatarsal1	Forefoot
TarsoMetatarsalDorsal3	Origin	Intermediate Cuneiform	Midfoot
	Insertion	Metatarsal2	Forefoot

Table B.5: Ligaments' geometry path - part 4.

Ligament	Point	Body	Model Segment
TarsoMetatarsalDorsal5	Origin	Lateral Cuneiform	Midfoot
	Insertion	Metatarsal3	Forefoot
TarsoMetatarsalDorsal7	Origin	Cuboid	Midfoot
	Insertion	Metatarsal4	Forefoot
TarsoMetatarsalDorsal8	Origin	Cuboid	Midfoot
	Insertion	Metatarsal5	Forefoot
TarsoMetatarsalPlantar1	Origin	Medial Cuneiform	Midfoot
	Insertion	Metatarsal1	Forefoot
TarsoMetatarsalPlantar2	Origin	Intermediate Cuneiform	Midfoot
	Insertion	Metatarsal2	Forefoot
TarsoMetatarsalPlantar3	Origin	Lateral Cuneiform	Midfoot
	Insertion	Metatarsal3	Forefoot
TarsoMetatarsalPlantar4	Origin	Cuboid	Midfoot
	Insertion	Metatarsal4	Forefoot
TarsoMetatarsalPlantar5	Origin	Cuboid	Midfoot
	Insertion	Metatarsal5	Forefoot

Appendix C

Abstract: CMBBE 2015

The abstract of the publication to be presented in the thirteenth International Symposium on Computer Methods in Biomechanics and Biomedical Engineering 2015 (CMBBE).

Development of a new CT scan based Foot-Ankle Multibody Model

Tiago M. Malaquias[1*], Carolina Silveira[2], Wouter Aerts[1], Friedl De Groote[3], Greta Dereymaeker[1], Jos Vander Sloten[1], Ilse Jonkers[4]
[1] Department of Mechanical Engineering, Biomechanical Section, KU Leuven, Belgium
[2]Department of Physics, University of Coimbra, Portugal
[3]Department of Mechanical Engineering, PMA, KU Leuven, Belgium
[4]Department of Kinesiology, Human Movement Biomechanics, KU Leuven, Belgium
*melo.malaquias@kuleuven.be

Introduction

Multibody simulations of human motion have been widely applied in the orthopedic field, i.e. to predict the outcome of medical treatments [1]. These methodologies require representative models for the anatomical structures. The foot, being a highly complex structure has been extensively described by simplified kinematic [2] and to a lesser extent dynamic models [1], [3], [4]. However, a model that fully captures the complexity of the foot is still lacking. In the present work, a simple semi-automated tool used to construct a new 3D multibody foot-ankle model based on CT scans is described. The model consists of five rigid segments (Talus, Calcaneus, Midfoot, Forefoot and Toes), connected using eleven degrees-of-freedom (DOF's), defined for use with inverse kinematics and inverse dynamic procedures in Opensim [5].

Methods

The semi-automated tool exists of a simple workflow that uses CT scans data to create the surfaces and volume meshes of both bones and soft tissue; From these, anatomical landmarks are selected, to allow the computation of the joint axes, segments origin as well as muscles and ligaments insertions [6]. The bone density is attributed according to the CT scans greyscale (in Hounsfield units) [7]. The soft tissue density is considered to be uniform (using *3-Matic®* and *Mimics®*). Based on this, the inertial properties, the total mass, the volume and the center of mass of each segment are computed [8] and assembled in an anthropometric datasheet (using *Matlab*). The model is then automatically generated using the *Matlab-OpenSim* interface. To test model performance, an integrated 3D gait analysis was used of one control subject, using the adapted marker set protocol of Duerinck by Burg [9]. This data was analyzed using inverse kinematic and inverse dynamic simulations in *OpenSim* [1].

Results

Joint angles and joint moments for five DOF's more specific the ankle, subtalar and metatarsophalangeal joints are shown in Fig. 1. Furthermore, some less commonly reported variables such as joint angles and moments at the Chopart's and tarsometatarsal joints are presented.

Conclusions

The proposed workflow allows the creation of a new generation of foot models that accurately represent the anatomical structure. The model-based inverse kinematic and inverse dynamic analysis of gait resulted in realistic kinematics and dynamics [4], [9]. Due to the more accurate representation of the degrees of freedom in the foot, this model has the potential to offer new insights in foot kinematics and dynamics. Future research will concentrate on updating the muscle and ligament parameters for use in forward simulations.

References

[1] S. L. Delp, et al., *IEEE Trans. Biomed. Eng.*, vol. 37, no. 8, pp. 757 – 767, 1990; [2] C. Bishop, et al., *J. Biomech.*, vol. 45, no. 13, pp. 2185–94, Aug. 2012; [3] F. C. Anderson and M. G. Pandy, *J. Biomech.*, vol. 34, pp. 153–161, 2001; [4] D. A. Bruening, et al., *Gait Posture*, vol. 35, no. 4, pp. 535–40, Apr. 2012; [5] S. L. Delp, et al., *IEEE Trans. Biomed. Eng.*, vol. 54, no. 11, pp. 1940–1950, 2007; [6] H. Kura, et al., *Anat. Rec.*, vol. 249, no. October 1996, pp. 143–151, 1997; [7] C. Bitsakos, et al., *J. Biomech.*, vol. 38, pp. 133–139, 2005; [8] F. Tonon, *J. Math. Stat.*, vol. 1, no. 1, pp. 8–11, 2004; [9] J. Burg, PhD Thesis, KU Leuven, 2014.

Figures

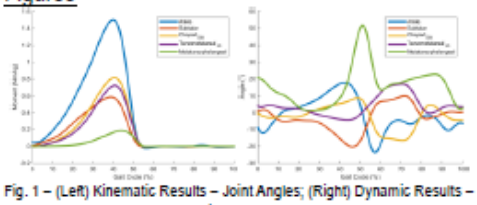

Fig. 1 – (Left) Kinematic Results – Joint Angles; (Right) Dynamic Results – Joint Torques.

Bibliography

[1] D. A. Winter. *Biomechanics and motor control of human movement*. 1990.

[2] Rosa Pàmies Vilà. *Application of Multibody Dynamics Techniques To The Analysis of Human Gait*. PhD thesis, Universitat Politècnica de Catalunya, 2012.

[3] E Muybridge. *Animal locomotion. An electro-photographic investigation of consecutive phases of animal movements.* Photogravure company of New York, University of Pennsylvania, New York, 1887.

[4] Simtk.org. OpenSim Project Overview. `https://simtk.org/home/opensim`. Date of access: 2015-05-22.

[5] Steven M Kidder, Faruk S Abuzzahab, Gerald F Harris, and Jeffrey E Johnson. A System for the Analysis of Foot and Ankle Kinematics During Gait. *EEE Transactions on Rehabilitation Engineering*, 4(1), 1996.

[6] Sylvain Carbes, Sø ren Tø rholm, Scott Telfer, Jim Woodburn, Michiel Oosterwaal, and John Rasmussen. A new multisegmental foot model and marker protocol for accurate simulation of the foot biomechanics during walking. *Proceedings of ISB 2011 Congress XXIII*, pages 1–2, 2011.

[7] Bruce A. MacWilliams, Matthew Cowley, and Diane E. Nicholson. Foot kinematics and kinetics during adolescent gait. *Gait and Posture*, 17(3):214–224, 2003.

[8] J. Stebbins, M. Harrington, N. Thompson, a. Zavatsky, and T. Theologis. Repeatability of a model for measuring multi-segment foot kinematics in children. *Gait and Posture*, 23(4):401–410, 2006.

[9] H. Cenk Güler, Necip Berme, and Sheldon R. Simon. A viscoelastic sphere model for the representation of plantar soft tissue during simulations. *Journal of Biomechanics*, 31(9):847–853, 1998.

[10] Nori Okita, Steven a. Meyers, John H. Challis, and Neil a. Sharkey. An objective evaluation of a segmented foot model. *Gait and Posture*, 30(1):27–34, 2009.

[11] J. H. Hicks. The mechanics of the foot. *Journal of anatomy*, 88(Pt 1):25–30.1, 1954.

[12] Michael Whittle. *Gait Analysis: An Introduction*. Butterworth-Heinemann, 2007.

[13] Richard D. Lannotti, Joseph P.; Parker. *The Netter collection of medical illustrations. 6: The musculoskeletal system Part 2: Spine and lower limb.* Philadelphia Elsevier Saunders, 2013.

[14] Henry Gray. Classification of Joints. In *Anatomy of the Human Body*, pages 1821–1865. 1918.

[15] C. H. Barnett and J. R. Napier. The axis of rotation at the ankle joint in man. *J. Anat. London*, (86):1–9, 1952.

[16] Shahan K. Sarrafian. *Anatomy of the Foot and Ankle. Descriptive, Topographic, Functional*. J. B. Lippincott Company, 1983.

[17] Yi-Chung Lin, Hyung Joo Kim, and Marcus G. Pandy. A computationally efficient method for assessing muscle funtion during human locomotion. *International Journal for Numerical Methods in Biomedical Engineering*, 27(1):436–449, 2011.

[18] Hideji Kura, Zong Ping Luo, Harold B. Kitaoka, and Kai Nan An. Quantitative analysis of the intrinsic muscles of the foot. *Anatomical Record*, 249(1):143–151, 1997.

[19] Pau Golanó, Jordi Vega, Peter a J de Leeuw, Francesc Malagelada, M. Cristina Manzanares, Víctor Götzens, and C. Niek van Dijk. Anatomy of the ankle ligaments: A pictorial essay. *Knee Surgery, Sports Traumatology, Arthroscopy*, 18(5):557–569, 2010.

[20] Josefien Burg. *Biomechanics of the foot-ankle complex before and after total ankle arthroplasty : An in vivo and in vitro analysis*. PhD thesis, KU Leuven, 2014.

[21] M. C. Carson, M. E. Harrington, N. Thompson, J. J. O'Connor, and T. N. Theologis. Kinematic analysis of a multi-segment foot model for research and clinical applications: A repeatability analysis. *Journal of Biomechanics*, 34(10):1299–1307, 2001.

[22] Uangthip Rattanaprasert, Richard Smith, Martin Sullivan, and Wendy Gilleard. Three-dimensional kinematics of the forefoot, rearfoot, and leg without the function of tibialis posterior in comparison with normals during stance phase of walking. *Clinical Biomechanics*, 14(1):14–23, 1999.

[23] Stephen C. Cobb, Laurie L. Tis, Jeffrey T. Johnson, Yong Tai Wang, Mark D. Geil, and Frances a. McCarty. The effect of low-mobile foot posture on multi-segment medial foot model gait kinematics. *Gait and Posture*, 30(3):334–339, 2009.

[24] Zimi Sawacha, Giuseppe Cristoferi, Gabriella Guarneri, Stefano Corazza, Giulia Donà, Paolo Denti, Andrea Facchinetti, Angelo Avogaro, and Claudio Cobelli. Characterizing multisegment foot kinematics during gait in diabetic foot patients. *Journal of Neuroengineering and Rehabilitation*, 6:37, 2009.

[25] Josh Tome, Deborah a Nawoczenski, Adolph Flemister, and Jeff Houck. Comparison of foot kinematics between subjects with posterior tibialis tendon dysfunction and healthy controls. *The Journal of Orthopaedic and Sports Physical therapy*, 36(9):635–644, 2006.

[26] A. Leardini, M. G. Benedetti, L. Berti, D. Bettinelli, R. Nativo, and S. Giannini. Rear-foot, mid-foot and fore-foot motion during the stance phase of gait. *Gait and Posture*, 25(3):453–462, 2007.

[27] Paolo Caravaggi, Claudia Giacomozzi, and Alberto Leardini. Foot segments mobility and plantar pressure in the normal foot. *Journal of Foot and Ankle Research*, 7(Suppl 1):A11, 2014.

[28] Ryan Mahaffey, Stewart C Morrison, Wendy I Drechsler, and Mary C Cramp. Evaluation of multi-segmental kinematic modelling in the paediatric foot using three concurrent foot models. *Journal of foot and ankle research*, 6(1):43, 2013.

[29] Stephen H. Scott and David a. Winter. Biomechanical model of the human foot: Kinematics and kinetics during the stance phase of walking. *Journal of Biomechanics*, 26(9):1091–1104, 1993.

[30] F.S. Abuzzahab, G.F. Harris, S.M. Kidder, and J.E. Johnson. A kinetic, biomechanical model of the foot and ankle. *Proceedings of 16th Annual International Conference of the IEEE Engineering in Medicine and Biology Society*, pages 0–1, 1994.

[31] Dustin a. Bruening, Kevin M. Cooney, and Frank L. Buczek. Analysis of a kinetic multi-segment foot model part II: Kinetics and clinical implications. *Gait and Posture*, 35(4):535–540, 2012.

[32] S. L. Delp, J. P. Loan, and M. G. Hoy. An interactive graphics-based model of the lower extremity to study orthopedic surgical procedures. *IEEE transactions on Biomedical Engineering*, 37(8):757–767, 1990.

[33] R. R. Neptune, I. C. Wright, and a. J. Van Den Bogert. A Method for Numerical Simulation of Single Limb Ground Contact Events: Application to Heel-Toe Running. *Computer Methods in Biomechanics and Biomedical Engineering*, 3(4):321–334, 2000.

[34] F C Anderson and M G Pandy. Dynamic optimization of human walking. *Journal of biomechanical engineering*, 123(5):381–390, 2001.

[35] AnyScript Community. The Glasgow-Maastricht Foot Model (FootGM), 2013. http://wiki.anyscript.org/index.php/AnyBody_Body_Model. Date of access: 2015-03-22.

[36] Scott L. Delp, Frank C. Anderson, Allison S. Arnold, Peter Loan, Ayman Habib, Chand T. John, Eran Guendelman, and Darryl G. Thelen. OpenSim: Open-source software to create and analyze dynamic simulations of movement. *IEEE Transactions on Biomedical Engineering*, 54(11):1940–1950, 2007.

[37] Cindy; Au and James Dunne. Gait 2392 and 2354 Models, 2013. http://simtk-confluence.stanford.edu:8080/display/OpenSim/Gait+2392+and+2354+Models. Date of access: 2015-06-26.

[38] Carl Gans. Fiber architecture and muscle function. *Exercise & Sport Science Reviews*, 10(1):160–207, 1982.

[39] Da Winter. *Biomechanics and motor control of human gait: normal, elderly and pathological*. 1991.

[40] P. Provenzano, R. Lakes, T. Keenan, and R. Vanderby. Nonlinear ligament viscoelasticity. *Annals of Biomedical Engineering*, 29(10):908–914, 2001.

[41] A Viidik. Simultaneous mechanical and light microscopic studies of collagen fibers. *Z Anat Entwicklungsgesch.*, 136(2):204–12, 1972.

[42] Albert L. Kwansa, Yvonne M. Empson, Emmanuel C. Ekwueme, Valerie I. Walters, Joseph W. Freeman, and Cato T. Laurencin. Novel matrix based anterior cruciate ligament (ACL) regeneration. *Soft Matter*, 6(20):5016, 2010.

[43] A/S AnyBody Technology. Anybody Tutorials - Lesson7: Ligaments. http://www.anybodytech.com/fileadmin/AnyBody/Docs/Tutorials/chap5_Muscle_modeling/lesson7.html. Date of access: 2015-03-06.

[44] J R Funk, G W Hall, J R Crandall, and W D Pilkey. Linear and quasi-linear viscoelastic characterization of ankle ligaments. *Journal of biomechanical engineering*, 122(1):15–22, 2000.

[45] Bernard Mengiardi, Marco Zanetti, Philip B Schöttle, Patrick Vienne, Beata Bode, Juerg Hodler, and Christian W a Pfirrmann. Spring ligament complex: MR imaging-anatomic correlation and findings in asymptomatic subjects. *Radiology*, 237(1):242–249, 2005.

[46] Clarissa Canella Moraes Do Carmo, Lina Isabel Fonseca De Almeida Melão, Marcio Freitas Valle De Lemos Weber, Debra Trudell, and Donald Resnick. Anatomical features of plantar aponeurosis: Cadaveric study using ultrasonography and magnetic resonance imaging. *Skeletal Radiology*, 37(10):929–935, 2008.

[47] Vishwas Patil, Nabil a Ebraheim, Alexandra Frogameni, and Jiayong Liu. Morphometric dimensions of the calcaneonavicular (spring) ligament. *Foot & ankle international / American Orthopaedic Foot and Ankle Society [and] Swiss Foot and Ankle Society*, 28(8):927–932, 2007.

[48] John Rule. Pictorial Essay Spring Ligament of the Ankle : Normal MR Anatomy. *American Journal of Roentgenology*, 161(6):1241–1244, 1993.

[49] Rita Stagni, Alberto Leardini, and Andrea Ensini. Ligament fibre recruitment at the human ankle joint complex in passive flexion. *Journal of Biomechanics*, 37(12):1823–1829, 2004.

[50] Jennifer Hicks. Marker (.trc) Files, 2013. `http://simtk-confluence.stanford.edu:8080/display/OpenSim/Marker+%28.trc%29+Files`. Date of access: 2015-06-26.

[51] Jennifer Hicks. How Scaling Works, 2015. `http://simtk-confluence.stanford.edu:8080/display/OpenSim/How+Scaling+Works`. Date of access: 2015-06-26.

[52] Christopher Hicks, Jennifer; Dembia. How to use the scale tool, 2013. `http://simtk-confluence.stanford.edu:8080/display/OpenSim/How+to+Use+the+Scale+Tool`. Date of access: 2015-06-26.

[53] F. De Groote, T. De Laet, I. Jonkers, and J. De Schutter. Kalman smoothing improves the estimation of joint kinematics and kinetics in marker-based human gait analysis. *Journal of Biomechanics*, 41(16):3390–3398, 2008.

[54] Christopher Hicks, Jennifer; Dembia. How Inverse Kinematics Works, 2013. `http://simtk-confluence.stanford.edu:8080/display/OpenSim/How+Inverse+Kinematics+Works`. Date of access: 2015-06-28.

[55] Jennifer Lund, Katherine; Hicks. Getting Started with Inverse Dynamics, 2012. `http://simtk-confluence.stanford.edu:8080/display/OpenSim/Getting+Started+with+Inverse+Dynamics`. Date of access: 2015-06-29.

[56] Jennifer Hicks. How Inverse Dynamics Works, 2012. `http://simtk-confluence.stanford.edu:8080/display/OpenSim/How+Inverse+Dynamics+Works`. Date of access: 2015-06-29.

[57] P. Lundgren, C. Nester, a. Liu, a. Arndt, R. Jones, a. Stacoff, P. Wolf, and a. Lundberg. Invasive in vivo measurement of rear-, mid- and forefoot motion during walking. *Gait and Posture*, 28(1):93–100, 2008.

[58] Wikipedia. Torque. `https://en.wikipedia.org/wiki/Torque`. Date of access: 2015-07-06.